The Astrophysical Journal, 808:148 (17pp), 2015 August 1 doi:10.1088/0004-637X/808/2/148

SYSTEMATIC Non-LTE STUDY OF THE $-2.6 \leqslant$ [Fe/H] $\leqslant 0.2$ F AND G DWARFS IN THE SOLAR NEIGHBORHOOD. I. STELLAR ATMOSPHERE PARAMETERS*

T. Sitnova[1,2,3], G. Zhao[1], L. Mashonkina[2], Y. Chen[1], F. Liu[1,4], Yu. Pakhomov[2], K. Tan[1], M. Bolte[5], S. Alexeeva[2], F. Grupp[6,7], J.-R. Shi[1], and H.-W. Zhang[8]
[1] Key Laboratory of Optical Astronomy, National Astronomical Observatories, Chinese Academy of Sciences, Beijing 100012, China; sitnova@inasan.ru
[2] Institute of Astronomy, Russian Academy of Sciences, RU-119017 Moscow, Russia
[3] Lomonosov Moscow State University, RU-119991 Moscow, Russia
[4] Research School of Astronomy and Astrophysics, Australian National University, Canberra, ACT 2611, Australia
[5] UCO/Lick Observatory, University of California, 1156 High Street, Santa Cruz, CA 95064, USA
[6] Universitats Sternwarte Munchen, Scheinerstrasse 1, D-81679 Munchen, Germany
[7] Max-Planck-Institut fur extraterrestrische Physik, Giessenbachstrasse, D-85748 Garching, Germany
[8] Department of Astronomy, School of Physics, Peking University, Beijing 100871, PR China
Received 2015 April 13; accepted 2015 June 3; published 2015 July 29

ABSTRACT

We present atmospheric parameters for 51 nearby F and G dwarf and subgiant stars uniformly distributed over the $-2.60 <$ [Fe/H] $< +0.20$ metallicity range that is suitable for the Galactic chemical evolution research. Lines of iron in the two ionization stages, Fe I and Fe II, were used to derive a homogeneous set of effective temperatures, surface gravities, iron abundances, and microturbulence velocities. Our spectroscopic analyses took advantage of employing high-resolution ($R \geqslant 60{,}000$) Shane/Hamilton and Canada–France–Hawaii Telescope/ESPaDOnS observed spectra and non-LTE (NLTE) line formation for Fe I and Fe II in the classical one-dimensional model atmospheres. The spectroscopic method was tested in advance with the 20 benchmark stars, for which there are multiple measurements of the infrared flux method effective temperature and their *Hipparcos* parallax error is less than 10%. We found NLTE abundances from lines of Fe I and Fe II to be consistent within 0.06 dex for every benchmark star, when applying a scaling factor of $S_{\rm H} = 0.5$ to the Drawinian rates of inelastic Fe+H collisions. The obtained atmospheric parameters were checked for each program star by comparing its position in the log g–$T_{\rm eff}$ plane with the theoretical evolutionary track of given metallicity and α-enhancement in the Yi et al. grid. Our final effective temperatures lie exactly in between the $T_{\rm IRFM}$ scales of Alonso et al. and Casagrande et al., with a mean difference of +46 and −51 K, respectively. NLTE leads to higher surface gravity compared with that for LTE. The shift in log g is smaller than 0.1 dex for stars with [Fe/H] $\geqslant -0.75$, $T_{\rm eff} \leqslant 5750$ K, or log $g \geqslant 4.20$. NLTE analysis is crucial for the very metal-poor turnoff and subgiant stars, for which the shift in log g between NLTE and LTE can be up to 0.5 dex. The obtained accurate atmospheric parameters will be used in the forthcoming papers to determine NLTE abundances of important astrophysical elements from lithium to europium and to improve observational constraints on the chemodynamical models of the Galaxy evolution.

Key words: stars: abundances – stars: atmospheres – stars: fundamental parameters

1. INTRODUCTION

In recent decades the construction of large telescopes, the developement of efficient spectrometers, and progress in stellar atmosphere and synthetic spectrum numerical modeling has provided a considerable improvement in the quality and quantity of stellar abundance determinations. Elemental abundances for the FGK-type stars provide important clues to understand the main processes at play in formation and evolution of the Milky Way (MW). Studies of stellar samples with metallicity[9] [Fe/H] $\geqslant -1$ showed how trends in various chemical elements can be used to learn the chemodynamical evolution of the Galactic disk (Edvardsson et al. 1993; Chen et al. 2000) and to resolve the thick disk and thin disk (Gratton et al. 1996; Fuhrmann 1998, 2004; Mashonkina & Gehren 2000; Reddy et al. 2003; Mishenina et al. 2004; Zhang & Zhao 2006; Adibekyan et al. 2013; Bensby et al. 2014, and references therein). Studies of very metal-poor (VMP, [Fe/H] $\leqslant -2$) stars unraveled the major processes of chemical enrichment of the MW (McWilliam et al. 1995; Cayrel et al. 2004; Zhang & Zhao 2005; Bonifacio et al. 2009).

Elemental abundances of stars with different metallicities are the main constraint for Galactic chemodynamical models (e.g., Chiappini et al. 2001; Romano et al. 2010; Kobayashi et al. 2011). For the Galactic chemical evolution research it would be useful to deal with a homogeneous set of accurate stellar abundances in a wide metallicity range, from supersolar down to extremely low iron abundances. Large high-resolution spectroscopic surveys were proposed to increase the statistics of observations and to improve a homogeneity of derived stellar chemical abundances over a wide metallicity range. The Apache Point Observatory Galactic Evolution Experiment (Zasowski 2013), with its 10^5 red giants observed in the near-infrared H band with a spectral resolving power of $R \simeq 22{,}500$, enables users to address numerous Galactic structure and stellar population issues. The *Gaia*-ESO Survey consortium (Gilmore et al. 2012; Randich & Gilmore 2013; Smiljanic et al. 2014) is obtaining high-quality spectroscopic data for about 10^5 stars using FLAMES at the Very Large Telescope (VLT). Spectra for a million stars will be acquired by the coming Galactic Archaeology with HERMES (GALAH) survey (De Silva et al. 2015).

* Based on observations collected at the UCO/Lick Observatory, USA, and Canada–France–Hawaii Telescope.
[9] In the classical notation, where $[{\rm X/H}] = \log(N_{\rm X}/N_{\rm H})_{\rm star} - \log(N_{\rm X}/N_{\rm H})_{\rm Sun}$.

We initiate a new project of deriving a homogeneous set of stellar atmosphere parameters and chemical abundances for the Galactic field FGK-type stars in the metallicity range $-3 \leqslant$ [Fe/H] $\leqslant +0.3$ that is suitable for a systematic research of Galactic chemical evolution. By employing high-resolution spectral observations, deriving accurate stellar atmosphere parameters, and treating the non-LTE (NLTE) line formation for the key chemical species, we attempt to push the accuracy of the abundance analysis to the points where the trends with metallicity could be meaningfully discussed. The selected stars are uniformly distributed in metallicity, and they can serve as a calibration sample for the existing and coming large-scale stellar surveys, such as the LAMOST Experiment for Galactic Understanding and Exploration (LEGUE; Deng et al. 2012), designed to determine from low-resolution spectra elemental abundances for hundreds of thousands to millions of stars, spread over much larger distances than ever before.

The goal of the present paper is the determination of precise atmospheric parameters, i.e., the effective temperature, $T_{\rm eff}$, the surface gravity, log g, the iron abundance, [Fe/H], and the microturbulence velocity, ξ_t, for the selected sample of, presumably, dwarf stars. The next papers in the series will be concerned with calculations of the NLTE abundances for many chemical elements from Li to Eu and analysis of the obtained abundance trends. Taking advantage of the Shane/Hamilton and Canada–France–Hawaii Telescope (CFHT)/ESPaDOnS high-resolution observational material with sufficient spectral coverage and the NLTE line formation for Fe I–Fe II, we determined stellar atmosphere parameters spectroscopically from lines of iron in the two ionization stages, Fe I and Fe II.

The spectroscopic methods are, in particular, useful for evaluating $T_{\rm eff}$ and log g of the VMP stars, which are mostly distant, and therefore their temperatures cannot be reliably derived from photometric colors owing to the uncertainty in the interstellar reddening data and, at present, surface gravities cannot be calculated from the trigonometric parallax because it is either rather uncertain or nonmeasurable. We look forward to seeing soon accurate parallaxes from *Gaia*.[10] In the literature there is no consensus on the validity of the excitation temperatures, $T_{\rm exc}$, derived through forcing no dependence of the Fe I line abundance on the excitation energy of the lower level, $E_{\rm exc}$. For their sample of VMP cool giants Cayrel et al. (2004) reached in LTE good agreement between the photometric and spectroscopic temperatures after they excluded strong lines with $E_{\rm exc} = 0$ eV. A similar approach (LTE, but not cutting $E_{\rm exc} = 0$ eV) yielded the same outcome for the VMP near-main-sequence stars in Frebel et al. (2013), while up to several hundred degrees cooler excitation temperatures than the photometric ones were found for the cool giants.

Ruchti et al. (2013) determined surface gravities of the stellar sample selected from the RAVE survey, using a grid of the NLTE abundance corrections from Lind et al. (2012). For common $T_{\rm eff}$ in the NLTE and LTE analysis, they found systematic biases in log g of up to 0.2 dex in the metallicity range $-2 <$ [Fe/H] < -0.5 and up to 0.3 dex for the more metal-poor stars.

The NLTE effects for lines of Fe I were accounted for by Bensby et al. (2014) in their study of 714 F and G dwarf stars, by applying the NLTE abundance corrections interpolated in the grid of Lind et al. (2012). They found minor shifts between NLTE and LTE, with $\Delta T_{\rm eff} = -12 \pm 28$ K, Δlog $g = +0.012 \pm 0.059$, and $\Delta \log \varepsilon$(Fe) $= -0.013 \pm 0.016$, on average. This is because the majority of their stars are close-to-solar-metallicity and mildly metal-deficient ones, with [Fe/H] > -1.2, and the NLTE abundance corrections are small, at the level of few hundredths, as predicted by Mashonkina et al. (2011) and Lind et al. (2012) for this metallicity range. Furthermore, the NLTE calculations of Lind et al. (2012) resulted in small departures from LTE for Fe I until extremely low metallicities because they were performed assuming a high efficiency of the Fe+H collisions and using the Drawinian rates (Drawin 1968, 1969). For nearby stars with very good *Hipparcos* parallaxes ($\Delta\pi/\pi < 0.05$), Bensby et al. (2014) found that essentially all stars with log $g > 4.2$ and $T_{\rm eff} < 5650$ K do not show ionization equilibrium between Fe I and Fe II, when determining the surface gravity from *Hipparcos* parallaxes. Bensby et al. (2014) suggested that classical plane-parallel one-dimensional (1D) models have limitations and cannot properly handle excitation balance and/or ionization balance, and they applied, therefore, empirical corrections to the atmospheric parameters from ionization balance. In this study we check with our stellar sample whether spectroscopic methods of $T_{\rm eff}$ and log g determination from lines of Fe I and Fe II have any limitations and what they are.

The paper is structured as follows. In Section 2 we describe the stellar sample, observations, and their reduction. Kinematical properties of the selected stars are calculated in Section 3. They are used to identify a membership of individual stars to the galactic stellar populations. Section 4 is concerned with the methodical issues. Stellar effective temperatures, surface gravities, iron abundances, microturbulence velocities, and masses are derived in Section 5. The obtained results are discussed in Section 6. Our conclusions are presented in Section 7.

2. STELLAR SAMPLE, OBSERVATIONS, SPECTRA REDUCTION

The stars were selected from the [Fe/H] catalog of Cayrel de Strobel et al. (2001) based on the following criteria.

1. The stars have a declination of $\delta > -20°$ to be observed at the nothern sky.
2. The selected stars should cover as broad as possible a metallicity range and be uniformly distributed, with two to three stars in each 0.1 dex metallicity interval.
3. The stellar sample should be homogeneous in temperature and luminosity. We selected the F-G-K dwarfs and subgiants based on the literature data.
4. Binaries, variables, and stars with any chemical peculiarity (carbon-enhanced stars, low [α/Fe] stars, etc.) were excluded.
5. For testing purposes the stellar sample should include a dozen well-studied stars of various metallicities, for which their stellar atmosphere parameters $T_{\rm eff}$ and log g were determined in the literature, presumably from the nonspectroscopic methods.

Thus, 50 stars, in total, were selected, and they cover the $-2.6 <$ [Fe/H] $< +0.3$ metallicity range.

Spectra of 48 stars were obtained using the Hamilton Echelle Spectrograph mounted on the Shane 3 m telescope of the Lick Observatory during the two observation runs 2011 March 15–16 and 2012 January 5–11. Most stars were observed at

[10] http://sci.esa.int/gaia/

Table 1
Abundance Differences Fe I–Fe II in the Selected Three Stars for Different Line Formation Scenarios

	LTE	NLTE		
HD		$S_H = 1$	$S_H = 0.5$	$S_H = 0.1$
84937	−0.06	−0.02	0.00	0.11
94028	−0.06	−0.05	−0.04	−0.01
140283	−0.06	−0.04	−0.02	0.10

least twice. The resolving power is $R = \lambda/\Delta\lambda \simeq 60{,}000$, and the spectral coverage is 3700–9300 Å. The signal-to-noise ratio (S/N) at 5500 Å is higher than 100 for most stars. The exception is BD −04° 3208, where S/N(λ = 5500 Å) ≃ 70. It is worth noting that the spectra suffer from the fringing effect in the infrared band.

For two stars, we used the spectra observed with the ESPaDOnS echelle spectrograph at the 3.6 m telescope of the Canada–France–Hawaii (CFH) observatory in queued service observing mode during several nights in 2011 and 2012. The spectra cover 3700–10450 Å. They have $R \simeq 81{,}000$ and $S/N \simeq 150$ at 5030 Å and a higher value of about 200 at 8090 Å.

The Shane/Hamilton spectra were reduced with the IRAF package following standard procedures that include the aperture definition, flat-field correction, background subtraction, 1D spectra extraction, wavelength calibration, and continuum normalization. The wavelength calibration was performed using the lamp with the titanium cathode in argon environment. Such a lamp is rare in the astronomical observations, and an appropriate list of the Ti and Ar lines was compiled by Pakhomov & Zhao (2013). The uncertainty in wavelength calibration is estimated to be 0.006 Å.

The CFHT/ESPaDOnS spectra were reduced with the special reduction package Libre-ESpRIT,[11] which includes two steps. The first one performs a geometrical analysis from a sequence of calibration exposures, and the second step achieves spectrum optimal extraction in itself, using the geometrical information derived in the first step. The reduction procedure returns the normalized spectra.

To improve the statistics of the VMP stars, we include the well-studied halo star HD 140283 in our sample. Its high-quality observed spectrum was taken from the ESO UVESPOP survey (Bagnulo et al. 2003). For seven stars our observational material was complemented with the data from different sources. We employed the spectra obtained by Klaus Fuhrmann with the fiber optics Cassegrain echelle spectrograph FOCES at the 2.2 m telescope of the Calar Alto Observatory from 1996 to 2000 (Fuhrmann 1998, 2004). The star BD − 04° 3208 was observed using UVES/VLT in 2001 April within our project 67.D-0086A (PI: T. Gehren). Details of spectra reduction were described by Mashonkina et al. (2003). For HD 49933 its high-quality spectrum was observed with the HARPS spectrograph at the 3.6 m ESO La Silla telescope. Details of spectra reduction were described by Ryabchikova et al. (2009).

This paper deals with 51 stars, in total. The investigated stars, together with characteristics of the observed spectra, are listed in Table 2.

[11] http://www.cfht.hawaii.edu/Instruments/Spectroscopy/Espadons

3. KINEMATIC PROPERTIES OF THE SELECTED STARS

The stellar kinematics is closely related to stellar populations in the Galaxy, and it is commonly applied to identify the membership of a given star to the galactic stellar populations, namely, the thin disk, the thick disk, and the halo.

The galactic space velocity components U, V, W were calculated using the equations and formalism of Johnson & Soderblom (1987). They were defined with respect to the local standard of rest (LSR), adopting the standard solar motion (U, V, W) = (10.00, 5.25, 7.17) km s^{-1} of Dehnen & Binney (1998). In computations of the X, Y, Z-coordinates, we used the best current estimate of the galactocentric distance of the Sun R_G = 8.0 kpc, which was inferred from a comparison of different statistical techniques (Malkin 2013). The parallaxes and proper motions were taken from the updated version of the *Hipparcos* catalog (van Leeuwen 2007) and the radial velocities from the *Hipparcos* Input catalog (Turon et al. 1993). The obtained results are presented in Table 3. The star BD −13°3442 is missing in the *Hipparcos* catalog, and it was assigned to the galactic halo based on its very low Fe abundance, with [Fe/H] = −2.62 (Section 5), and high proper motion as indicated by the SIMBAD database.[12]

Following Fuhrmann (2000) and later studies (e.g., Chen et al. 2004; Bensby et al. 2010), we identify the stars with peculiar space velocities with respect to the LSR in the range 85 km s^{-1} < v_{pec} < 180 km s^{-1} as belonging to the thick-disk stellar population, the stars with v_{pec} < 85 km s^{-1} to the thin disk, and all the halo stars of our sample have v_{pec} > 200 km s^{-1} (Figure 1). The star G090-003 is not shown in Figure 1, because its peculiar space velocity, v_{pec} = 847 ± 1580 km s^{-1}, is rather uncertain owing to the large error of the *Hipparcos* parallax, π = 1.12 ± 2.14 mas. For six stars with peculiar space velocities close to v_{pec} = 85 km s^{-1}, their membership to either the thin disk or the thick disk cannot be decided using only the kinematic properties. Following Fuhrmann (1998), we also took into account their chemical properties, as determined in Section 5. For example, HD 30562, with v_{pec} = 93 km s^{-1}, was assigned to the thin disk because it has a supersolar Fe abundance, with [Fe/H] = 0.17, and it does not reveal Mg enhancement relative to Fe.

4. METHOD OF CALCULATIONS

Stellar parameters of the selected sample were determined in this study applying different methods, including the spectroscopic one based on the NLTE analysis of lines of Fe I and Fe II. This section describes calculations of the theoretical spectra.

4.1. Codes and Model Atmospheres

The statistical equilibrium (SE) of Fe I–Fe II was calculated with a comprehensive model atom treated by Mashonkina et al. (2011). The main source of the uncertainty in the NLTE results for Fe I is poorly known inelastic collisions with hydrogen atoms. We employed the formula of Drawin (1968, 1969), as implemented by Steenbock & Holweger (1984), for allowed $b - b$ and $b - f$ transitions and a simple relation between hydrogen and electron collisional rates, $C_H = C_e\sqrt{(m_e/m_H)}N_H/N_e$, for forbidden transitions, following Takeda (1994). Mashonkina et al. (2011) recommended to

[12] http://simbad.u-strasbg.fr/simbad/

Table 2
Characteristics of Observed Spectra

HD,BD	V	[Fe/H]	S/N	t_{exp}, s	N_{spec}	Date (yyyy mm dd)
			Shane/Hamilton			
19373	4.05	0.10	234, 228	30.00, 30.00	2	2012 Jan 09, 2012 Jan 09
22484	4.28	0.01	171, 160	30.00, 30.00	2	2012 Jan 09, 2012 Jan 09
22879	6.74	−0.84	170, 195	360.00, 360.00	2	2012 Jan 09, 2012 Jan 09
24289	9.96	−1.94	112, 128	2700.00, 2700.00	2	2012 Jan 09, 2012 Jan 09
30562	5.77	0.17	180, 190	120.00, 120.00	2	2012 Jan 09, 2012 Jan 09
30743	6.26	−0.44	188, 184	240.00, 240.00	2	2012 Jan 09, 2012 Jan 09
34411	4.70	0.01	220, 218, 209F[a]	45.00, 45.00, 84.19	3	2012 Jan 11, 2012 Jan 11, 2012 Jan 07
43318	5.65	−0.19	210, 212, 183F	100.00, 100.00, 215.14	3	2012 Jan 11, 2012 Jan 11, 2012 Jan 07
45067	5.90	−0.16	230, 235	180.00, 180.00	2	2012 Jan 09, 2012 Jan 09
45205	8.00	−0.87	140, 177	1200.00, 1800.00	2	2012 Jan 09, 2012 Jan 09
49933	5.78	−0.47	216, 203	659.71, 135.0	2	2012 Jan 08, 2012 Jan 10
52711	5.93	−0.21	256, 163F	160.00, 119.18	2	2012 Jan 10,2012 Jan 06
58855	5.36	−0.29	224, 167F	150.00, 75.13	2	2012 Jan 09, 2012 Jan 06
59374	8.50	−0.88	122F, 131F	1174.47, 812.31	2	2012 Jan 07, 2012 Jan 06
59984	5.93	−0.69	182F, 165F	269.17, 229.17	2	2012 Jan 07, 2012 Jan 06
62301	6.75	−0.70	197, 158F	450.00, 238.20	2	2012 Jan 09, 2012 Jan 06
64090	8.30	−1.73	280, 136F	2500.00, 687.35	2	2012 Dec 26, 2012 Jan 06
69897	5.10	−0.25	186, 180F	240.00, 66.18	2	2012 Jan 08, 2012 Jan 06
74000	9.67	−1.97	144, 142, 74F	2400.00, 2400.00, 1454.51	3	2012 Jan 10, 2012 Jan 10, 2012 Jan 06
76932	5.86	−0.98	170, 181F, 210F	612.32, 258.23, 489.24	3	2012 Jan 08, 2012 Jan 06, 2012 Jan 07
82943	6.54	0.19	214, 170F	270.00, 342.25	2	2012 Jan 10, 2012 Jan 06
84937	8.28	−2.16	122, 153, 95	1475.81, 1800.0, 846.41	3	2012 Jan 08, 2012 Jan 09, 2012 Jan 06
89744	5.74	0.13	220, 165F	135.00, 121.16	2	2012 Jan 10, 2012 Jan 06
90839	4.83	−0.18	190, 169F	60.00, 137.20	2	2012 Jan 10, 2012 Jan 06
92855	7.28	−0.12	171, 163F	600.00, 309.20	2	2012 Jan 10, 2012 Jan 06
94028	8.23	−1.47	118, 172	1800.00, 1317.69	2	2011 Mar 15, 2011 Mar 15
99984	5.95	−0.38	181F, 183F	517.22, 491.24	2	2012 Jan 07, 2012 Jan 07
100563	5.70	0.06	171F, 173F	413.25, 383.21	2	2012 Jan 07, 2012 Jan 07
102870	3.61	0.11	208F, 211F	77.12, 91.13	2	2012 Jan 07, 2012 Jan 07
103095	6.45	−1.26	188	300.00	1	2012 Jan 10
105755	8.59	−0.73	175, 103F	2400.0, 1052.44	2	2012 Jan 10, 2012 Jan 06
106516	6.11	−0.73	151F, 155F	434.25, 546.25	2	2012 Jan 07, 2012 Jan 07
108177	9.66	−1.67	60, 111	3000.00, 3600.00	2	2011 Mar 15, 2011 Mar 15
110897	6.00	−0.57	260, 170F, 172F	600.00, 568.30, 508.23	3	2012 Jan 08, 2012 Jan 07, 2012 Jan 07
114710	4.26	0.06	184F, 186F	112.13, 129.15	2	2012 Jan 07, 2012 Jan 07
115617	4.74	−0.10	177, 170	160.00, 160.00	2	2012 Jan 08, 2012 Jan 08
134088	8.00	−0.80	130	1800.00	1	2011 Mar 15
134169	7.67	−0.78	214, 212	750.00, 750.00	2	2012 Jan 10, 2012 Jan 10
138776	8.72	0.24	211	1800.00	1	2012 Jan 11
142091	4.82	−0.07	277, 275	60.00, 60.00	2	2012 Jan 11, 2012 Jan 11
142373	4.62	−0.54	140, 147	240.00, 240.00	2	2012 Jan 08, 2012 Jan 08
−04°3208	9.99	−2.20	60, 66	1500.00, 2400.00	2	2012 Jan 08, 2012 Jan 08
−13°3442	10.37	−2.62	103, 102, 104, 102	2700.00, 2700.00, 2700.00, 2700.00	4	2012 Jan 09, 2012 Jan 09, 2012 Jan 09, 2012 Jan 09
+24°1676	10.80	−2.44	86, 90, 92, 92, 57F	2400.00, 2400.00, 2400.00, 2400.00, 1581.60	5	2012 Jan 11, 2012 Jan 11, 2012 Jan 11, 2012 Jan 11, 2012 Jan 06
+29°2091	10.22	−1.91	82, 121, 115, 120, 83F	2400.00, 2700.00, 2700.00, 2700.00, 1287.46	5	2012 Jan 08, 2012 Jan 10, 2012 Jan 10, 2012 Jan 10, 2012 Jan 06
+37°1458	8.92	−1.95	235, 105F	2500.00, 897.38	2	2012 Jan 10, 2012 Jan 06
+66°0268	9.88	−2.06	112, 110, 115	2400.00, 2400.00, 2400.00	3	2012 Jan 10, 2012 Jan 10, 2012 Jan 10
G090-003	10.50	−2.04	106, 120, 122, 66F	2700.00, 2700.00, 2700.00, 1181.44	4	2012 Jan 11, 2012 Jan 11, 2012 Jan 11, 2012 Jan 06
			CFHT/ESPaDOnS			
+07°4841	10.38	−1.46	152	1470	2	⋯
+09°0352	10.17	−2.09	160	2400	2	⋯
			FOCES			
22879	6.74	−0.84	200	900.00, 1800.00, 1800.00	3	1996 Sep 02, 1999 Jan 02, 1996 Dec 31
34411	4.70	0.01	200	1500.00, 1500.00	2	1999 Aug 21, 1998 Dec 27
84937	8.28	−2.16	200	3600.00, 3300.00	2	1999 Mar 01, 1999 Mar 01
94028	8.23	−1.47	200	2400.00, 2400.00	2	2000 Jan 17, 2000 Jan 17
103095	6.45	−1.26	200	900.00	1	2000 May 19
142373	4.62	−0.54	200	600.00, 600.00	2	1998 Jun 09, 1998 Jun 09
			Others			

Table 2
(Continued)

HD,BD	V	[Fe/H]	S/N	t_{exp}, s	N_{spec}	Date (yyyy mm dd)
49933[b]	4.15	−0.47	500	...	...	...
140283[c]	7.21	−2.46	200	...	...	...
−04° 3208[c]	9.99	−2.20	200	...	...	...

Notes.
[a] F indicates the observations carried out by Debra Fischer.
[b] 3.6 m/HARPS.
[c] VLT/UVES.

scale the Drawin rates by a factor of $S_H = 0.1$ based on their analysis of element abundances derived from the two ionization stages, Fe I and Fe II, in the selected VMP stars. Bergemann et al. (2012) estimated a larger value of $S_H = 1$. In this study, S_H was further constrained using the benchmark stars.

The coupled radiative transfer and SE equations were solved with a revised version of the DETAIL code (Butler & Giddings 1985). The update was presented by Mashonkina et al. (2011). The obtained departure coefficients were then used by the codes binmag3 (Kochukhov 2010), synthV-NLTE (V. Tsymbal 2015, private communication, based on SynthV code; Tsymbal et al. 1996), and SIU (Reetz 1991) to calculate the synthetic line profiles.

We used the MARCS model structures (Gustafsson et al. 2008),[13] which were interpolated for given T_{eff}, log g, and [Fe/H] using a FORTRAN-based routine written by Thomas Masseron.[14]

4.2. Selection of Iron Lines

The investigated lines were selected according to the following criteria.

i. The lines should be almost free of visible/known blends in the solar spectrum.
ii. For Fe I the line list should cover a range of excitation energies of the lower level, E_{exc}, as large as possible to investigate the excitation equilibrium of neutral iron. On the other hand, the low-excitation ($E_{exc} < 1.2$ eV) lines in metal-poor stars often appear to have higher abundances than lines with higher excitation energy (see, e.g., Cayrel et al. 2004; Lai et al. 2008). The calculations with ab initio 3D, time-dependent, hydrodynamical model atmospheres of cool stars predict that the 3D effects for lines of Fe I are strongly E_{exc} dependent (Collet et al. 2007; Dobrovolskas et al. 2013). For example, the 3D abundance corrections amount to −0.8 and −0.25 dex for the $E_{exc} = 0$ lines of Fe I in the models T_{eff}/log g/[M/H] = 5860/4/−2 and 5850/4/−1, respectively, while they are −0.2 and −0.07 dex for the $E_{exc} = 2$ eV lines and close to 0 for the $E_{exc} = 4$ eV lines (Dobrovolskas et al. 2013). To minimize a possible influence of the 3D effects on T_{eff} determinations, we did not consider lines of Fe I with $E_{exc} < 2$ eV.
iii. For both close-to-solar-metallicity and VMP stars, lines of various strength have to be present in the spectrum to evaluate stellar microturbulence velocity ξ_t.

[13] http://marcs.astro.uu.se
[14] http://marcs.astro.uu.se/software.php

For individual stars, we also avoided using saturated lines with the equivalent width EW > 180 mÅ to minimize the influence of a possible uncertainty in the van der Waals damping constants on final abundances.

The selected lines are listed in Table 4 along with their atomic parameters. For neutral iron we employed experimental gf-values from Blackwell et al. (1979, 1982a, 1982b), O'Brian et al. (1991), and Bard et al. (1991). Two sets of oscillator strengths from Meléndez & Barbuy (2009) and Raassen & Uylings (1998) were inspected for Fe II. Van der Waals broadening of the selected lines is accounted for using the most accurate data as provided by Barklem et al. (2000) for Fe I and Barklem & Aspelund-Johansson (2005) for Fe II.

4.3. Sun as a Reference Star

To minimize the effect of the uncertainty in gf-values on the final results, we applied a line-by-line differential NLTE and LTE approach, in the sense that stellar line abundances were compared with individual abundances of their solar counterparts. The solar flux observations were taken from the Kitt Peak Solar Flux Atlas (Kurucz et al. 1984). The calculations were performed with the MARCS model atmosphere 5777/4.44/0. A microturbulence velocity of 0.9 km s^{-1} was adopted.

The solar LTE and NLTE abundances from individual lines are presented in Table 4. The NLTE calculatoins were performed using S_H= 0.5 (see Section 5). For the Fe I lines, the solar mean LTE and NLTE abundances are log $A_{LTE} = -4.57 \pm 0.09$ and log $A_{NLTE} = -4.56 \pm 0.09$. Hereafter, $A_X = N_X/N_{tot}$ is the element abundance taken relative to the total number of atoms. For lines of Fe II, the NLTE abundance corrections do not exceed 0.01 dex, in absolute value, and the solar mean abundance amounts to $\log A = -4.56 \pm 0.05$ and $\log A = -4.50 \pm 0.05$, when using gf-values from Meléndez & Barbuy (2009) and Raassen & Uylings (1998), respectively. Hereafter, the statistical abundance error is the dispersion in the single line measurements about the mean: $\sigma = \sqrt{\Sigma(x - x_i)^2/(N-1)}$, where N is the total number of lines used, x is their mean abundance, and x_i is the individual abundance of each line. It is worth noting that an uncertainty of 0.06 dex in abundance from the Fe II lines leads to a 0.12 dex uncertainty in log g for solar-type stars. This is crucial for surface gravity determinations from the Fe I/Fe II ionization equilibrium.

5. DETERMINATION OF STELLAR PARAMETERS

To derive atmospheric parameters of our stellar sample, the following strategy was applied. First, we selected the stars, for which their effective temperatures and surface gravities were

Table 3
Stellar Kinematics and Membership to Particular Galactic Stellar Population

HD, BD	X-8000 (pc)	Y (pc)	Z (pc)	U (km s^{-1})	V (km s^{-1})	W (km s^{-1})	[Mg/Fe] NLTE	Stellar Population
19373	10	−10	−1	−75.2	−16.1	21.5	0.00 ± 0.03	Thin disk
22484	10	0	−9	1.7	−15.5	−42.3	−0.05 ± 0.02	Thin disk
22879	20	0	−17	−109.9	−88.2	−41.3	0.30 ± 0.02	Thick disk
24289	160	30	−139	−116.7	−172.6	173.9	0.21 ± 0.04	Halo
30562	20	10	−13	−54.9	−72.0	−21.6	0.04 ± 0.05	Thin disk
30743	20	20	−18	24.8	−5.2	−22.5	0.08 ± 0.06	Thin disk
34411	10	0	0	−74.5	−35.4	4.4	−0.03 ± 0.03	Thin disk
43318	30	20	−5	47.0	1.2	−37.0	−0.05 ± 0.05	Thin disk
45067	30	20	−3	−16.5	−64.4	13.7	0.01 ± 0.04	Thin disk
45205	60	−30	26	−35.9	−89.5	17.0	0.39 ± 0.03	Thick disk
49933	30	20	0	25.7	−13.1	−9.2	0.16 ± 0.10	Thin disk
52711	20	0	5	−18.6	−77.8	−9.0	0.01 ± 0.05	Thin disk
58855	20	0	9	25.3	−15.4	−3.9	0.07 ± 0.03	Thin disk
59374	40	20	14	−48.5	−120.3	−9.8	0.30 ± 0.02	Thick disk
59984	20	20	3	8.0	−11.4	−21.2	0.10 ± 0.02	Thin disk
62301	30	0	16	−7.4	−110.0	−22.1	0.26 ± 0.03	Thick disk
64090	30	0	13	266.9	−227.6	−89.6	0.24 ± 0.04	Halo
69897	20	0	9	−23.9	−38.7	7.1	−0.01 ± 0.06	Thin disk
74000	60	110	34	216.8	−348.0	62.2	0.37 ± 0.03	Halo
76932	10	20	7	−49.1	−91.3	70.0	0.32 ± 0.05	Thick disk
82943	10	20	13	13.3	−13.5	−12.6	−0.05 ± 0.05	Thin disk
84937	40	30	52	205.0	−214.7	−7.9	0.21 ± 0.08	Halo
89744	20	0	33	−10.6	−29.9	−14.3	−0.02 ± 0.04	Thin disk
90839	10	0	10	−13.9	−1.8	2.4	0.02 ± 0.03	Thin disk
92855	20	0	32	−42.1	−22.4	−13.9	−0.02 ± 0.04	Thin disk
94028	20	10	42	−33.7	−129.3	13.5	0.35 ± 0.05	Thick disk
99984	20	−10	49	−6.4	11.0	−36.1	0.02 ± 0.03	Thin disk
100563	0	10	24	−14.5	−20.9	−9.8	−0.03 ± 0.03	Thin disk
102870	0	10	10	40.4	3.2	7.3	−0.02 ± 0.03	Thin disk
103095	0	0	9	278.3	−157.2	−14.8	0.24 ± 0.06	Halo
105755	30	−30	78	26.7	5.3	8.3	0.34 ± 0.08	Thin disk
106516	0	10	18	53.4	−73.4	−57.7	0.38 ± 0.04	Thick disk
108177	−20	50	99	126.7	−262.9	32.0	0.23 ± 0.04	Halo
110897	0	0	17	−41.7	7.0	75.3	0.18 ± 0.03	Thin disk
114710	0	0	9	−49.9	11.5	8.4	−0.07 ± 0.04	Thin disk
115617	0	0	6	−23.3	−47.8	−31.3	−0.10 ± 0.02	Thin disk
134088	−30	0	26	−25.6	−72.4	−68.7	0.36 ± 0.03	Thick disk
134169	−40	0	44	2.5	−3.3	−1.9	0.32 ± 0.02	Thin disk
138776	−50	0	45	6.4	−56.4	−5.0	0.02 ± 0.04	Thin disk
140283	−50	0	32	−249.0	−253.3	41.1	0.23 ± 0.03	Halo
142091	−10	−20	24	33.6	−40.7	-18.1	0.07 ± 0.05	Thin disk
142373	0	−10	12	−41.6	10.8	−68.3	0.18 ± 0.01	Thin disk
−04° 3208	−30	110	169	−123.5	−309.9	−120.2	0.21 ± 0.06	Halo
−13° 3442							0.23 ± 0.01	Halo
+07° 4841	−50	−150	−123	−224.4	−283.9	−55.3	0.43 ± 0.05	Halo
+09° 0352	120	−40	−120	−156.5	−176.9	97.7	0.45 ± 0.05	Halo
+24° 1676	360	90	126	166.8	−483.7	106.4	0.21 ± 0.06	Halo
+29° 2091	40	20	85	157.3	−345.9	88.4	0.34 ± 0.04	Halo
+37° 1458	150	−10	26	−280.3	−233.0	−26.0	0.38 ± 0.05	Halo
+66° 0268	40	−40	10	−181.0	−426.4	−73.1	0.15 ± 0.07	Halo
G090-003	820	90	332	10.4	−824.6	−192.4	0.25 ± 0.05	Halo

determined reliably using the nonspectroscopic methods, namely, $T_{\rm eff}$ from the infrared flux method (IRFM) and log g from the well-known relation between log g, stellar mass M, $T_{\rm eff}$, and absolute bolometric magnitude $M_{\rm bol}$:

$$[g] = [M] + 4[T_{\rm eff}] + 0.4(M_{\rm bol} - M_{\rm bol\odot}). \quad (1)$$

Here square brackets denote the logarithmic ratio with respect to the solar value. The $M_{\rm bol}$ magnitudes were obtained using the V magnitudes from Olsen (1983, 1993), the revised *Hipparcos* parallaxes of van Leeuwen (2007), and the bolometric corrections (BCs) from Alonso et al. (1995). For the Sun the absolute visual magnitude $M_{V\odot} = 4.87$ and $\mathrm{BC}_\odot = -0.12$ were adopted. The star's mass was estimated from its position in the $M_{\rm bol}$–log $T_{\rm eff}$ diagram by interpolating in the Dartmouth isochrones (Dotter et al. 2008). "Reliably" means that multiple measurements of the IRFM temperature are available and the uncertainty in the *Hipparcos*-parallax-based surface gravity, log $g_{\rm Hip}$, is less than 0.1 dex. This implies a

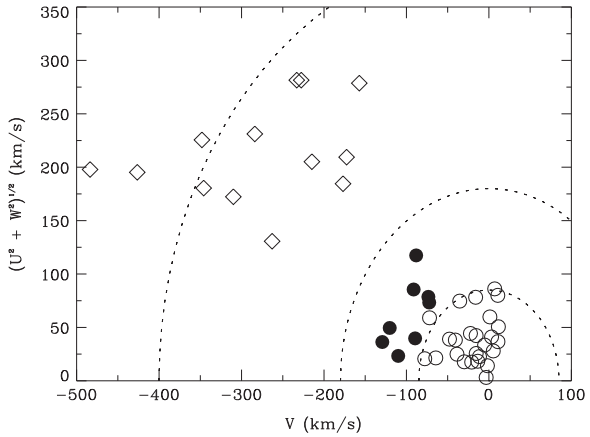

Figure 1. Toomre diagram for the investigated stars from the perspective of the LSR. Dashed curves delineate constant peculiar space velocities $v_{\rm pec} = (U^2 + V^2 + W^2)^{1/2} = 85$, 180, and 400 km s^{-1}. Different symbols show the thin disk (open circles), thick disk (filled circles), and halo (open diamonds) stars.

parallax error of smaller than 10%. A total of 20 stars in our sample meet these requirements. They are listed in Table 5 as the benchmark stars.

Atmospheric parameters of the remaining stars were derived or improved spectroscopically from the NLTE analysis of lines of Fe I and Fe II. In the stellar parameter range, with which we are concerned, lines of Fe I are weakened toward higher $T_{\rm eff}$, resulting in higher derived element abundance, while they are nearly insensitive to variation in log g. In contrast, lines of Fe II are only weakly sensitive to variation in $T_{\rm eff}$, while they are weakened with log g increasing. If $T_{\rm eff}$ is fixed, the surface gravity is obtained from the requirement that abundances from lines of Fe I and Fe II must be equal. One needs to be cautious when deriving both $T_{\rm eff}$ and log g from Fe I and Fe II. Any shift in $T_{\rm eff}$ leads to shifting log g in the sense that an increase in $T_{\rm eff}$ leads to an increase in log g. Therefore, in this study we used nonspectroscopic (IRFM) determinations of $T_{\rm eff}$, where available, and for every star its final parameters, $T_{\rm eff}$/log g/[Fe/H], were checked with the corresponding evolutionary track.

For each benchmark star, abundances from lines of Fe I and Fe II were derived under various line-formation assumptions, i.e., NLTE with $S_{\rm H} = 0.1$, 0.5, 1 and LTE, and we investigated which of them lead to consistent element abundances from both ionization stages. Our calculations showed that the departures from LTE are small for the [Fe/H] > -1 stars. Indeed, in this metallicity range the NLTE abundance correction, $\Delta_{\rm NLTE} = \log A_{\rm NLTE} - \log A_{\rm LTE}$, does not exceed 0.04 dex for $S_{\rm H} = 0.5$, and the difference in NLTE abundances between $S_{\rm H} = 0.1$ and 0.5 is smaller than 0.04 dex. Three of six [Fe/H] < -1 stars are cool, with $T_{\rm eff} \leqslant 5400$ K, and they are not useful for constraining $S_{\rm H}$ because of small $\Delta_{\rm NLTE} \leqslant 0.02$ dex. Table 1 lists the abundance differences between Fe I and Fe II from the calculations with different $S_{\rm H}$ for the three benchmark stars with the largest NLTE effects. For every star, the acceptable abundance difference is achieved with $S_{\rm H} = 0.5$ and 1. Hereafter, we choose $S_{\rm H} = 0.5$ to perform the NLTE calculations for Fe I–Fe II.

Spectroscopic stellar parameters were obtained in the iterative procedure. For each star, our initial guess was $T_{\rm eff} = T_{\rm IRFM}$, if available, or $T_{\rm eff} = T_{b-y}$ and log g = log $g_{\rm Hip}$. Effective temperature and surface gravity were corrected until the ionization equilibrium between Fe I and Fe II and the Fe I excitation equilibrium were fulfilled.

Table 4
Line Data, Iron NLTE and LTE Abundances from an Analysis of the Solar Spectrum, and Equivalent Widths (EW) of the Solar Lines

λ, Å	$E_{\rm exc}$ (eV)	log gf	log C_6	log A NLTE	log A LTE	EW (mÅ)
Fe I						
4920.50	2.83	0.07	−30.51	−4.61	−4.61	466.0
5198.72	2.22	−2.14	−31.32	−4.52	−4.53	102.0
5217.40	3.21	−1.07	−30.37	−4.57	−4.57	130.3
5232.94	2.94	−0.06	−30.54	−4.68	−4.68	371.1
5236.20	4.19	−1.50	−31.32	−4.68	−4.69	33.7
5242.50	3.63	−0.97	−31.56	−4.47	−4.47	93.4
5281.79	3.04	−0.83	−30.53	−4.68	−4.69	163.6
5324.18	3.21	−0.10	−30.42	−4.54	−4.54	332.5
5367.47	4.41	0.44	−30.20	−4.78	−4.78	170.1
5379.58	3.69	−1.51	−31.56	−4.46	−4.47	64.1
5383.37	4.31	0.64	−30.37	−4.72	−4.72	220.5
5393.17	3.24	−0.72	−30.42	−4.60	−4.60	171.2
5491.83	4.19	−2.19	−31.33	−4.53	−4.54	14.5
5586.76	3.37	−0.10	−30.38	−4.58	−4.58	289.3
5662.52	4.18	−0.57	−30.52	−4.41	−4.42	105.7
5696.09	4.55	−1.72	−30.21	−4.68	−4.69	14.6
5705.46	4.30	−1.36	−30.47	−4.61	−4.62	41.2
5778.45	2.59	−3.44	−31.37	−4.60	−4.61	22.7
5855.08	4.61	−1.48	−30.21	−4.58	−4.59	24.4
5916.25	2.45	−2.99	−31.45	−4.43	−4.44	56.7
6065.49	2.61	−1.53	−31.41	−4.51	−4.52	132.1
6082.71	2.22	−3.57	−31.74	−4.55	−4.56	34.7
6151.62	2.18	−3.30	−31.58	−4.52	−4.53	51.1
6200.32	2.61	−2.44	−31.43	−4.47	−4.48	74.6
6213.43	2.22	−2.48	−31.58	−4.58	−4.59	86.0
6229.23	2.85	−2.80	−31.32	−4.65	−4.66	37.8
6252.55	2.40	−1.69	−31.52	−4.52	−4.53	135.4
6393.61	2.43	−1.43	−31.53	−4.63	−4.64	150.8
6411.65	3.65	−0.60	−30.38	−4.57	−4.57	154.7
6421.35	2.28	−2.03	−31.80	−4.56	−4.57	112.7
6518.37	2.83	−2.46	−31.37	−4.59	−4.60	64.0
Fe II						
4233.17	2.58	−1.97	−32.01	−4.64	−4.64	132.1
4508.29	2.84	−2.44	−32.00	−4.48	−4.48	93.0
4582.83	2.83	−3.18	−32.03	−4.54	−4.54	57.7
4620.52	2.82	−3.21	−32.02	−4.63	−4.63	53.9
4923.93	2.88	−1.26	−32.03	−4.69	−4.69	196.1
5018.44	2.88	−1.10	−32.04	−4.72	−4.72	219.1
5197.58	3.22	−2.22	−32.02	−4.58	−4.58	85.4
5264.81	3.22	−3.13	−32.01	−4.48	−4.48	49.2
5284.11	2.88	−3.11	−32.04	−4.57	−4.57	60.3
5325.55	3.21	−3.16	−32.03	−4.55	−4.55	45.2
5414.07	3.21	−3.58	−32.02	−4.52	−4.52	29.8
5425.26	3.20	−3.22	−32.04	−4.56	−4.56	43.4
5991.38	3.15	−3.55	−32.05	−4.58	−4.58	32.1
6239.95	3.89	−3.46	−32.00	−4.55	−4.55	13.2
6247.56	3.89	−2.30	−32.00	−4.58	−4.58	55.0
6369.46	2.89	−4.11	−32.06	−4.59	−4.59	20.7
6432.68	2.89	−3.57	−32.07	−4.56	−4.56	43.2
6456.38	3.90	−2.05	−32.00	−4.59	−4.59	66.9

Note. The gf-values are from Blackwell et al. (1979, 1982a, 1982b), O'Brian et al. (1991), and Bard et al. (1991) for Fe I and from Meléndez & Barbuy (2009) for Fe II.

Table 5
Final Stellar Parameters

HD, BD	$T_{\rm eff}$ (K)	log g	[Fe/H]	ξ_t (km s^{-1})	Mass ($M_\odot$)	Fe I–Fe II LTE	Fe I–Fe II NLTE	$N_{\rm Fe\,I}$	$N_{\rm Fe\,II}$
				Benchmark stars					
19373	6045 ± 80	4.24 ± 0.05	0.10 ± 0.05	1.2	1.11	0.06 ± 0.09	0.06 ± 0.09	26	15
22484	6000 ± 100	4.07 ± 0.05	0.01 ± 0.04	1.1	1.18	−0.02 ± 0.07	0.00 ± 0.07	27	16
22879	5800 ± 90	4.29 ± 0.07	−0.84 ± 0.07	1.0	0.75	−0.06 ± 0.08	−0.03 ± 0.08	23	14
30562	5900 ± 85	4.08 ± 0.05	0.17 ± 0.08	1.3	1.12	0.02 ± 0.09	0.02 ± 0.09	26	16
34411	5850 ± 100	4.23 ± 0.05	0.01 ± 0.03	1.2	1.10	−0.01 ± 0.05	−0.02 ± 0.05	26	15
49933	6600 ± 80	4.15 ± 0.05	−0.47 ± 0.07	1.7	1.11	−0.05 ± 0.08	−0.04 ± 0.08	26	15
59374	5850 ± 55	4.38 ± 0.09	−0.88 ± 0.05	1.2	0.75	−0.06 ± 0.09	−0.02 ± 0.09	24	15
59984	5930 ± 100	4.02 ± 0.06	−0.69 ± 0.07	1.4	0.89	−0.06 ± 0.10	−0.06 ± 0.10	23	18
64090	5400 ± 70	4.70 ± 0.08	−1.73 ± 0.07	0.7	0.62	−0.02 ± 0.09	−0.02 ± 0.09	22	11
69897	6240 ± 70	4.24 ± 0.05	−0.25 ± 0.04	1.4	1.15	−0.06 ± 0.07	−0.04 ± 0.07	28	15
84937	6350 ± 85	4.09 ± 0.08	−2.12 ± 0.07	1.7	0.76	−0.06 ± 0.11	0.00 ± 0.12	12	7
94028	5970 ± 130	4.33 ± 0.08	−1.47 ± 0.04	1.3	0.70	−0.06 ± 0.07	−0.04 ± 0.07	20	15
102870	6170 ± 80	4.14 ± 0.04	0.11 ± 0.06	1.5	1.35	−0.03 ± 0.07	−0.01 ± 0.07	23	14
103095	5130 ± 65	4.66 ± 0.08	−1.26 ± 0.08	0.9	0.60	0.01 ± 0.11	0.01 ± 0.11	22	8
105755	5800 ± 55	4.05 ± 0.09	−0.73 ± 0.05	1.2	0.85	−0.01 ± 0.06	0.00 ± 0.06	23	15
114710	6090 ± 80	4.47 ± 0.05	0.06 ± 0.06	1.1	1.17	0.03 ± 0.07	0.04 ± 0.06	26	15
134169	5890 ± 80	4.02 ± 0.07	−0.78 ± 0.07	1.2	0.87	0.01 ± 0.09	0.06 ± 0.09	26	18
140283	5780 ± 55	3.70 ± 0.07	−2.46 ± 0.07	1.6	0.80	−0.06 ± 0.09	−0.02 ± 0.09	20	14
142091	4810 ± 65	3.12 ± 0.06	−0.07 ± 0.10	1.2	1.16	0.05 ± 0.13	0.05 ± 0.12	20	13
+66° 0268	5300 ± 80	4.72 ± 0.11	−2.06 ± 0.15	0.6	0.60	−0.03 ± 0.16	−0.03 ± 0.16	21	9
				Stars with Spectroscopic Parameters					
24289	5980	3.71	−1.94 ± 0.17	1.1	0.83	−0.10 ± 0.19	−0.03 ± 0.19	16	10
30743	6450	4.20	−0.44 ± 0.07	1.8	1.08	−0.03 ± 0.09	0.01 ± 0.09	26	18
43318	6250	3.92	−0.19 ± 0.08	1.7	1.26	−0.05 ± 0.13	−0.01 ± 0.09	28	15
45067	5960	3.94	−0.16 ± 0.06	1.5	1.18	−0.03 ± 0.07	−0.01 ± 0.07	24	16
45205	5790	4.08	−0.87 ± 0.03	1.1	0.82	−0.08 ± 0.07	−0.05 ± 0.07	23	16
52711	5900	4.33	−0.21 ± 0.05	1.2	0.97	0.03 ± 0.07	0.05 ± 0.07	26	16
58855	6410	4.32	−0.29 ± 0.05	1.6	1.15	−0.01 ± 0.08	0.01 ± 0.07	26	15
62301	5840	4.09	−0.70 ± 0.04	1.3	0.85	−0.07 ± 0.08	−0.04 ± 0.08	29	16
74000	6225	4.13	−1.97 ± 0.07	1.3	0.76	−0.08 ± 0.10	−0.02 ± 0.10	15	7
76932	5870	4.10	−0.98 ± 0.05	1.3	·	−0.01 ± 0.07	0.03 ± 0.08	27	16
82943	5970	4.37	0.19 ± 0.04	1.2	1.17	0.01 ± 0.06	0.01 ± 0.06	25	13
89744	6280	3.97	0.13 ± 0.03	1.7	1.50	0.01 ± 0.05	0.02 ± 0.06	26	13
90839	6195	4.38	−0.18 ± 0.05	1.4	1.10	0.04 ± 0.07	0.06 ± 0.07	28	17
92855	6020	4.36	−0.12 ± 0.03	1.3	1.08	0.00 ± 0.06	0.02 ± 0.05	24	11
99984	6190	3.72	−0.38 ± 0.04	1.8	1.33	−0.01 ± 0.07	0.03 ± 0.07	24	15
100563	6460	4.32	0.06 ± 0.08	1.6	1.30	0.00 ± 0.10	0.02 ± 0.10	23	10
106516	6300	4.44	−0.73 ± 0.06	1.5	0.95	−0.03 ± 0.08	0.00 ± 0.08	22	15
108177	6100	4.22	−1.67 ± 0.05	1.1	0.72	−0.08 ± 0.13	−0.06 ± 0.14	16	5
110897	5920	4.41	−0.57 ± 0.04	1.2	0.85	0.03 ± 0.05	0.05 ± 0.05	29	18
115617	5490	4.40	−0.10 ± 0.05	1.1	0.93	−0.04 ± 0.08	−0.05 ± 0.08	26	13
134088	5730	4.46	−0.80 ± 0.05	1.1	0.75	−0.02 ± 0.07	0.00 ± 0.07	25	15
138776	5650	4.30	0.24 ± 0.05	1.3	0.93	0.02 ± 0.10	0.00 ± 0.10	21	11
142373	5830	3.96	−0.54 ± 0.05	1.4	0.95	−0.02 ± 0.07	−0.02 ± 0.07	28	17
−4° 3208	6390	4.08	−2.20 ± 0.09	1.4	0.77	−0.08 ± 0.11	0.00 ± 0.11	16	11
−13° 3442	6400	3.95	−2.62 ± 0.09	1.4	0.79	−0.14 ± 0.11	0.00 ± 0.11	8	5
+7° 4841	6130	4.15	−1.46 ± 0.05	1.3	0.79	0.00 ± 0.09	0.02 ± 0.08	21	17
+9° 0352	6150	4.25	−2.09 ± 0.04	1.3	0.70	−0.01 ± 0.07	0.03 ± 0.07	15	6
+24° 1676	6210	3.90	−2.44 ± 0.09	1.5	0.78	−0.06 ± 0.12	0.04 ± 0.12	12	5
+29° 2091	5860	4.67	−1.91 ± 0.08	0.8	0.70	−0.05 ± 0.10	−0.05 ± 0.10	18	10
+37° 1458	5500	3.70	−1.95 ± 0.09	1.0	·	−0.07 ± 0.11	−0.05 ± 0.11	21	14
G090-003	6010	3.90	−2.04 ± 0.06	1.3	0.78	−0.06 ± 0.10	−0.02 ± 0.10	17	12

5.1. Effective Temperatures

Although there are multiple measurements of the IRFM effective temperature for individual stars of our sample (Alonso et al. 1996a; González Hernández & Bonifacio 2009; Casagrande et al. 2010, 2011), we found no study that provides the data for every investigated star. Figure 2 (top panel) displays the differences between different sources for the stars in common with this work. It can be seen that the $T_{\rm eff}$ scale of Casagrande et al. (2011, hereafter C11) is hotter than that of Alonso et al. (1996a, hereafter A96), with $\Delta T_{\rm IRFM}$(C11–A96) = 114 ± 62 K for 25 stars. The difference between C11 and González Hernández and Bonifacio (2009, hereafter GB09) is smaller, $\Delta T_{\rm IRFM}$(C11–GB09) = 32 ± 83 K for 26 stars. Here we did not count the two outliers HD 34411 and HD 142373, with large uncertainties in $T_{\rm IRFM}$ of 479 and 342

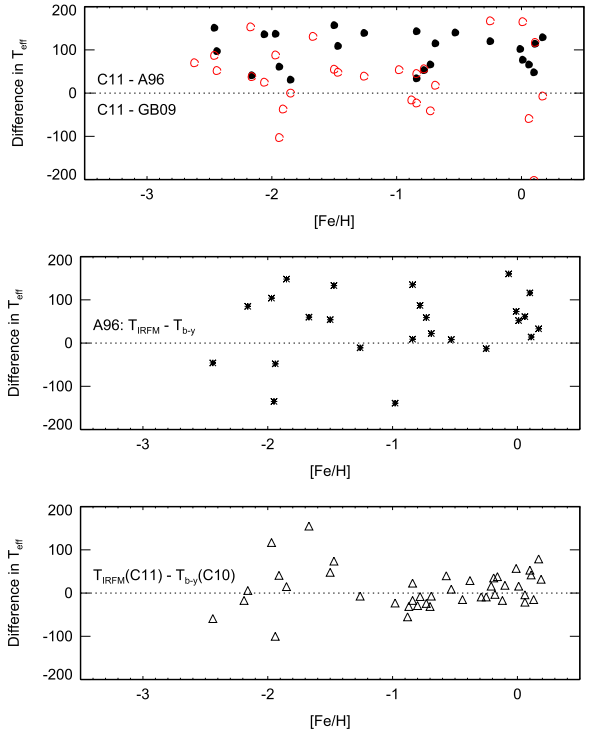

Figure 2. Top panel: differences in the IRFM effective temperatures of the investigated stars between Casagrande et al. (2011, C11) and Alonso et al. (1996a, A96; filled circles) and between C11 and González Hernández & Bonifacio (2009, GB09; open circles). Middle panel: differences $T_{\rm IRFM}$(A96)–T_{b-y} (Alonso et al. 1996b). Bottom panel: differences $T_{\rm IRFM}$(C11)–T_{b-y} (Casagrande et al. 2010, C10).

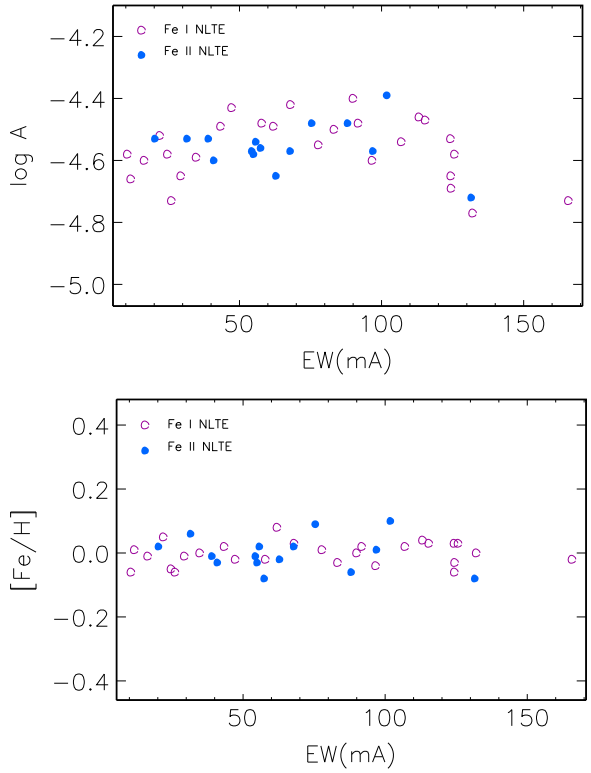

Figure 3. Absolute (top panel) and differential (bottom panel) NLTE abundances from lines of Fe I (open circles) and Fe II (filled circles) in HD 22484.

K, respectively, which were caused by using saturated Two Micron All Sky Survey (2MASS) photometry.

We calculated four sets of the photometric temperatures from the $b-y$ and $V-K$ color indices using two different calibrations of Casagrande et al. (2010, hereafter C10) and Alonso et al. (1996b). The V magnitudes and $b-y$ colors were taken from Olsen (1983, 1993) for 45 stars, in total, and the K magnitudes from the 2MASS catalog (Skrutskie et al. 2006) for 24 stars, in total. Figure 2 display the differences between $T_{\rm IRFM}$ and T_{b-y} for both effective temperature scales. We found that T_{b-y} and T_{V-K} agree well with those from the IRFM, when using the calibrations of C10, with $T_{\rm IRFM}$ (C11) – T_{b-y}(C10) = 10 ± 46 K (42 stars) and $T_{\rm IRFM}$ (C11) – T_{V-K} (C10) = 22 ± 68 K (21 stars). For the Alonso et al. (1996b) calibration, the differences are larger, with $T_{\rm IRFM}$ (A96) – T_{b-y} = 41 ± 78 K (25 stars) and $T_{\rm IRFM}$ (A96) – T_{V-K} = 72 ± 58 K (12 stars), although the statistics is small for the $V-K$ photometry.

For the *benchmark stars*, we aimed to have a homogeneous set of $T_{\rm eff}$ based on a single source of the IRFM temperatures. The only study that provides $T_{\rm IRFM}$ for every benchmark star is GB09. Using their $T_{\rm IRFM}$, we could not achieve the Fe I/Fe II ionization equilibrium and the Fe I excitation equilibrium for half of the benchmark stars, independent of applying either the LTE or NLTE approach. No preference was therefore given to any source of $T_{\rm IRFM}$. Instead, for each star its temperature from A96, GB09, C10, and C11, where available, and the corresponding log $g_{\rm Hip}$ value were checked with the difference in NLTE abundances between Fe I and Fe II and a slope of the [Fe/H] versus $E_{\rm exc}$ plot for Fe I. For six stars, corrections up to 50 K were applied to the most appropriate $T_{\rm IRFM}$ to obtain the final effective temperature (Table 5).

5.2. Surface Gravities, Metallicities, and Microturbulence Velocities

For each benchmark star, the NLTE abundances from the two ionization stages, Fe I and Fe II, were found to be consistent within 0.06 dex. Hereafter, 0.06 dex is considered as an admissible difference between Fe I and Fe II, when deriving spectroscopic stellar parameters of the remaining, non-benchmark stars. For a given star, we started from checking the photometric temperature, $T_{\rm IRFM}$ or T_{b-y}, and the *Hipparcos*-parallax-based gravity, log $g_{\rm Hip}$. Effective temperature and surface gravity were allowed to vary within the corresponding error bars. The procedure was iterated until the NLTE abundance difference Fe I–Fe II is smaller than 0.06 dex, the excitation trend for Fe I disappears, and lines of different equivalent width give consistent iron abundances.

We found that the differential approach largely removes a line-to-line scatter for the [Fe/H] $\geqslant -1.5$ stars. For example, when moving from the absolute to the differential NLTE abundances, the dispersion reduces from $\sigma = 0.10$ dex to $\sigma = 0.04$ dex for lines of Fe I and from $\sigma = 0.08$ dex to $\sigma = 0.05$ dex for lines of Fe II in HD 22484 (6000/4.07/0.01; Figure 3). For more metal-poor stars, the differential approach is less efficient in removing a line-to-line scatter. For example, for HD 84937 (6350/4.09/–2.12) the scatter of data reduces for Fe II but not Fe I lines (Figure 4). When using the $E_{\rm exc} > 2$ eV lines of Fe I, we obtained $\sigma = 0.035$ and 0.078 dex for the absolute and differential abundances, respectively. This is probably due to the uncertainties in the

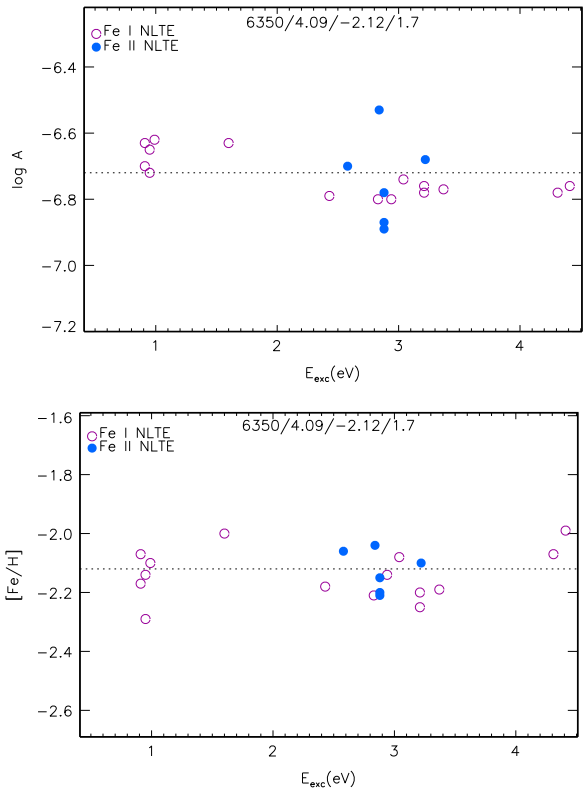

Figure 4. Absolute (top panel) and differential (bottom panel) NLTE abundances from lines of Fe I (open circles) and Fe II (filled circles) in HD 84937.

van der Waals damping constant, C_6. The lines, which can be measured in the VMP stars, have strong van der Waals broadened wings in the solar spectrum (for example, Fe I λ5383; Figure 5). For such a line, the uncertainty in the derived solar abundance is contributed from the uncertainties in both *gf*- and C_6-values. When dealing with the VMP stars, the differential analysis is able to cancel the uncertainty in *gf*, but not C_6.

Although our final results are based on using the $E_{\rm exc} \geqslant 2$ eV lines of Fe I, for most stars we also checked abundances determined from the lower-excitation lines. We found no abundance difference between the low- and high-excitation lines for close-to-solar-metallicity stars. For the most metal-poor stars, such as HD 84937, the absolute abundances reveal an excitation trend, but it disappears for the differential abundances (Figure 4).

We did not determine stellar parameters under the LTE assumption and cannot evaluate the differences in log *g* between using LTE and NLTE. However, the NLTE effects can be estimated based on our LTE and NLTE calculations for Fe I–Fe II and the sensitivity of iron lines to variation in log *g*. Since the departures from LTE lead to weakened lines of Fe I, but they do not affect lines of Fe II until the extremely low metallicities, the ionization equilibrium Fe I/Fe II is achieved for higher gravities in NLTE than in LTE. The shifts in log *g* increase toward lower metallicity and surface gravity. For our program stars they may be up to 0.1 dex at [Fe/H] > -1.5, up to 0.2 dex for $-2.2 <$ [Fe/H] < -1.8, and reach 0.45 dex for the most metal-poor star of our sample, BD −13° 3442, with [Fe/H] = –2.62.

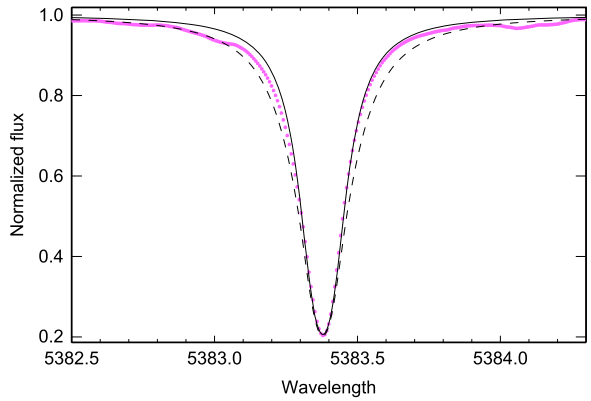

Figure 5. Theoretical NLTE profiles of Fe I λ5383 computed with $\log C_6 = -30.370$ (Barklem et al. 2000; dashed curve) and $\log C_6 = -31.095$ (Kurucz 2007; solid curve) compared to the solar spectrum (Kurucz et al. 1984; bold dots). Everywhere in the calculations, $\log A_{\rm Fe} = -4.54$. To fit the solar line profile with $\log C_6 = -30.370$, one needs to reduce the iron abundance down to $\log A_{\rm Fe} = -4.72$.

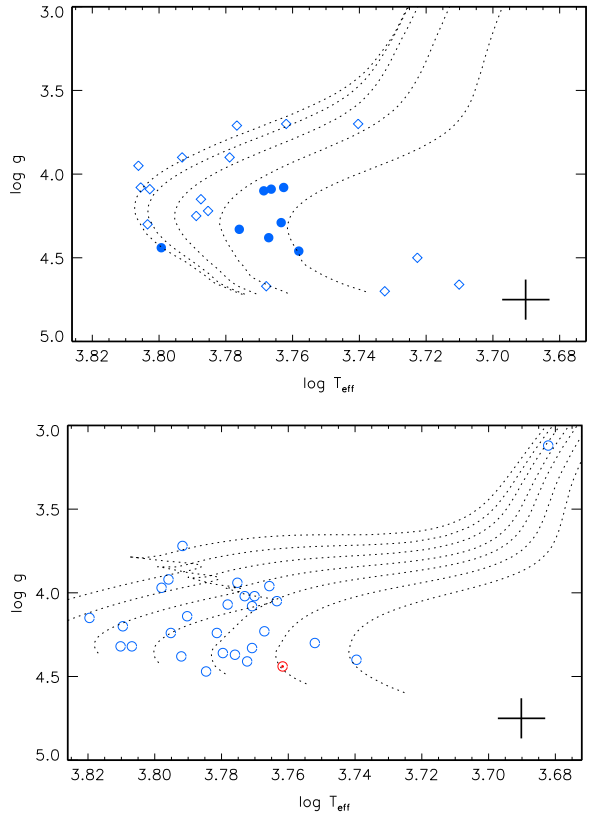

Figure 6. Top panel: investigated thick-disk (filled circles) and halo (diamonds) stars compared with the evolutionary tracks of $M = 0.75\,M_\odot$ and [Fe/H] from –2.75 to –0.75 (from left to right), with a step of 0.5 dex. Bottom panel: thin-disk stars (open circles) compared with the evolutionary tracks of the solar metallicity and the stellar mass varying between $M = 0.9\,M_\odot$ and $1.5\,M_\odot$, with a step of $0.1 M_\odot$. The crosses in each panel indicate log *g* and $T_{\rm eff}$ error bars of 0.12 dex and 80 K, respectively.

5.3. Checking Atmospheric Parameters with Evolutionary Tracks

For each star the obtained effective temperature and surface gravity were checked by comparing its position in the log *g* – $T_{\rm eff}$ plane with the theoretical evolutionary track of given metallicity and α-enhancement in the Yi et al. (2004) grid

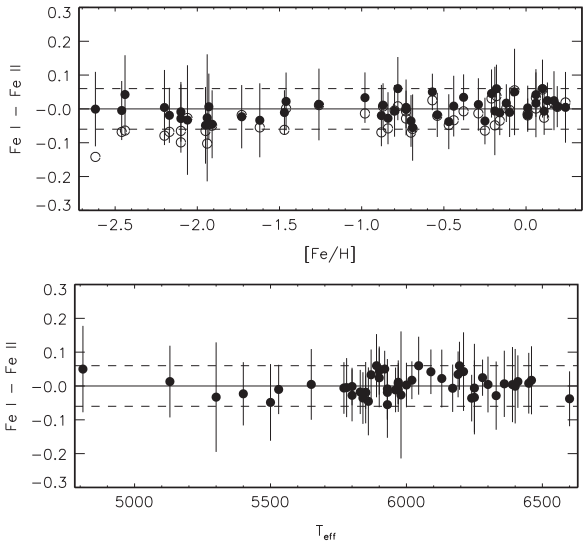

Figure 7. NLTE (filled circles) and LTE (open circles, top panel only) abundance differences Fe I–Fe II for the investigated stars. Dashed lines indicate an admissible difference of ±0.06 dex.

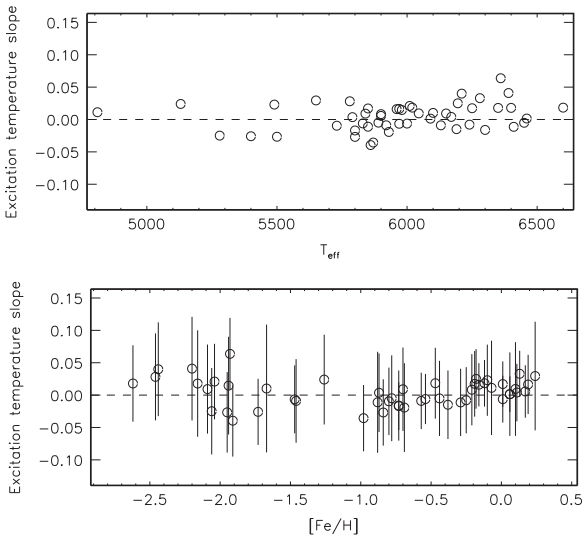

Figure 8. Excitation temperature slopes from Fe I lines for the investigated stars.

(Figure 6). An α-enhancement was assumed to be equal to [Mg/Fe] as derived in this study and presented in Table 3. Stellar masses corresponding to the best-fit evolutionary tracks are indicated in Table 5. They range between 0.60 and 0.85 solar mass for the halo and thick-disk stars, which does not contradict their evolutionary status and old age. For the thin-disk stars, their masses range between 0.85 $M_{\odot}$ and 1.5 $M_{\odot}$ and ages between 1 and 9 Gyr.

For two halo cool dwarfs we had to revise $T_{\rm eff}$/log g, to force the stars to sit on the main sequence of the appropriate evolutionary track. We stress that the changes in atmospheric parameters were not allowed to destroy the ionization equilibrium between Fe I and Fe II and the Fe I excitation equilibrium. For HD 64090, we adopted $T_{\rm eff}$= 5400 K, which is close to $T_{\rm IRFM}$ = 5440 K (A96), and log g = 4.70, which is $1.5\sigma_{\log\ g}$ higher than log $g_{\rm Hip}$. For BD +66°0268 our final temperature, $T_{\rm eff}$= 5300 K, is close to $T_{\rm IRFM}$ = 5280 K (A96), and log g = 4.72 is $2\sigma_{\log\ g}$ higher than log $g_{\rm Hip}$.

5.4. Final Atmospheric Parameters

The final atmospheric parameters, together with the NLTE and LTE abundance differences between Fe I and Fe II, are presented in Table 5. For the star's metallicity we adopted [Fe/H] determined from lines of Fe II, although the difference in NLTE abundances between Fe I and Fe II nowhere exceeds 0.06 dex. The Fe I–Fe II abundance differences are also shown in Figure 7. In NLTE, they reveal no trends with any atmospheric parameter, either [Fe/H], or $T_{\rm eff}$, or log g.

Figure 8 displays the excitation temperature slopes, d[Fe/H]/$d\ E_{\rm exc}$, calculated from lines of Fe I in the individual stars. The data reveal no trend with effective temperature, and d[Fe/H]/$dE_{\rm exc}$ = 0.0044 dex/eV, on average. The excitation slope seems to depend slightly on metallicity at [Fe/H] $\geqslant -1$, although nowhere does its magnitude exceed the error bars. The scatter of data is larger for the [Fe/H] < -1.8 than less metal-poor stars owing to the smaller number of observed lines of Fe I.

In Figure 9 we compare surface gravities from the Fe I/Fe II NLTE ionization equilibrium and *Hipparcos* parallax methods for the 20 stars that do not belong to the benchmark stellar

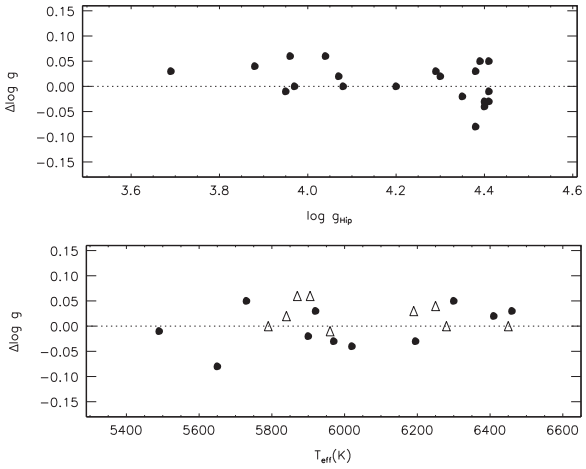

Figure 9. Differences in surface gravity from the Fe I/Fe II NLTE ionization equilibrium and *Hipparcos* parallax methods for 20 stars with the spectroscopically derived atmospheric parameters and a relative parallax uncertainty less than 10%. In the bottom panel, the filled circles and open triangles show stars with log $g_{Hip} > 4.2$ and $\leqslant 4.2$, respectively.

sample but have a relative parallax uncertainty less than 10%. The differences are minor, with Δlog g(Sp–Hip) = 0.008 ± 0.037 dex, on average, and they do not show any trends with surface gravity or effective temperature. Having in mind that for each benchmark star the Fe I/Fe II ionization equilibrium was achieved with log g from the *Hipparcos* parallax method, we infer that the spectroscopic method of gravity determination is working in the 5130 K $\leqslant T_{\rm eff} \leqslant$ 6600 K and 3.12 $\leqslant$ log $g \leqslant$ 4.66 range. An exception is HD 64090, for which we determined log $g_{\rm Sp}$ = 4.70, which is 0.13 dex higher than log $g_{\rm Hip}$. We thus do not confirm a temperature trend of Δlog g (Sp–Hip) for cool ($T_{\rm eff} < 5300$ K) dwarf (log $g > 4.2$) stars obtained by Bensby et al. (2014).

Final slopes of the [Fe/H] versus EW plots amount to –0.0002 dex/mÅ, on average. Using the derived microturbulence velocities ξ_t and basic atmosheric parameters $T_{\rm eff}$, log g,

and [Fe/H], we built up the approximation formula:

$$\xi_t = -0.21 + 0.06 \times [\mathrm{Fe/H}] + 5.6 \times \left(T_{\rm eff}/10^4\right) - 0.43 \times \log\ g. \quad (2)$$

Microturbulence velocity grows toward higher $T_{\rm eff}$ and lower surface gravity. The metallicity dependence is weak. Similar relations were previously found by other authors, for example, Nissen (1981), Edvardsson et al. (1993), Allende Prieto et al. (2004), and Ramírez et al. (2013). In the first three studies their formulae did not include the [Fe/H] term because these studies dealt with the limited metallicity range. Using Equation (2) results in $\xi_t = 1.1$ and 1.4 km s^{-1} for the solar atmospheric parameters and 6000/4.0/−1.0, respectively. For comparison, the corresponding values are 1.1 and 1.5 km s^{-1} from the Ramírez et al. (2013) formula.

5.5. Notes on Individual Stars

We provide additional comments on stars that turned out to be interesting for one or another reason in the course of the analysis.

HD 59984 and HD 105755, with [Fe/H] = −0.69 and −0.73, respectively, may be the most metal-poor thin-disk stars. Both kinematics, $v_{\rm pec}$ = 25 and 28 km s^{-1}, and an age of 8 Gyr for both stars support their thin-disk status.

HD 106516: we failed to obtain self-consistent stellar parameters for this star. On the one hand, the star exhibits a typical thick-disk kinematics, $v_{\rm pec}$ = 108 km s^{-1}, and chemical signatures, [Mg/Fe] = 0.38 and [Fe/H] = −0.73. On the other hand, its age was estimated to be 6 Gyr and unlikely older than 9 Gyr, identifying the star as a thin-disk star. According to Carney et al. (2001), it is a single-lined spectroscopic binary, with the period P = 843.9 days.

HD 134169: kinematics, $v_{\rm pec}$ = 5 km s^{-1}, identifies it as a thin-disk star. However, HD 134169 exhibits typical thick-disk chemical signatures, [Mg/Fe] = 0.32 and [Fe/H] = −0.78, and old age, $\tau \simeq$ 11 Gyr. Enhancement of Al relative to Fe, with [Al/Fe] = 0.54, found by Gehren et al. (2006) also suggests a thick-disk origin.

BD +37° 1458: this is a halo star. With spectroscopic $T_{\rm eff}$ = 5500 K, log g = 3.70, and [Fe/H] = −1.95, the star sits on the evolutionary track of $M = 0.67 M_\odot$ at τ = 24 Gyr. The younger age can only be obtained for higher $T_{\rm eff}$ and log g. However, there is no ground for a substantial revision of atmospheric parameters. The star's temperature is well fixed by several studies. Alonso et al. (1996a), Ramírez & Meléndez (2005), and González Hernández & Bonifacio (2009) derived $T_{\rm IRFM}$ = 5510, 5516, and 5582 K, respectively. Axer et al. (1994) determined $T_{\rm eff}$ = 5450 K from the Balmer line wing fits. With $T_{\rm eff}$ = 5500 K, log $g_{\rm Hip}$ = 3.41 ± 0.18 is even lower than the spectroscopically derived value. For this star we choose the spectroscopic stellar parameters as the final ones.

5.6. Uncertainties in Derived Atmospheric Parameters

The following approaches were applied to evaluate the uncertainties in the derived atmospheric parameters.

For the benchmark stars we adopted the $T_{\rm IRFM}$ errors as indicated by the original sources. Statistical error of the *Hipparcos*-parallax-based surface gravity was computed as the quadratic sum of errors of the star's parallax, effective temperature, mass, visual magnitude, and BC:

$$\sigma^2_{\log\ g} = \left(2\sigma_{\log \pi}\right)^2 + \left(4\sigma_{\log T}\right)^2 + \sigma^2_{\log M} + \left(0.4\sigma_V\right)^2 + \left(0.4\sigma_{\rm BC}\right)^2.$$

The uncertainties in V magnitude and BC together contribute less than 0.01 dex to the total log g error. For $T_{\rm eff}$ the contribution nowhere exceeds 0.03 dex. Stellar masses were well constrained using the evolutionary tracks, with an uncertainty of no more than 0.1 $M_\odot$, resulting in 0.04 dex contribution to $\sigma_{\log\ g}$.

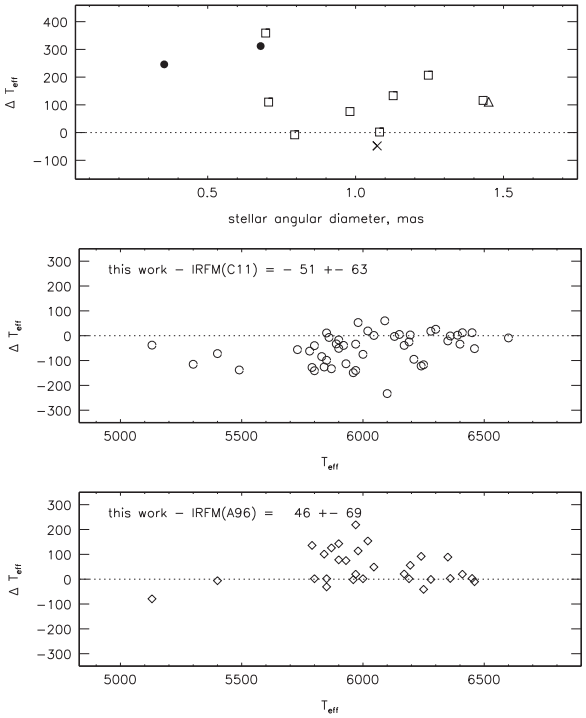

Figure 10. Differences in effective temperature between this study and the literature data. The top panel corresponds to interferometric measurements of Boyajian et al. (2012, 2013; squares), Creevey et al. (2012, 2015; filled circles), North et al. (2009; triangle), and von Braun (2014; cross). See Section 6 for more details. The middle and bottom panels use the IRFM temperatures from Casagrande et al. (2011) and Alonso et al. (1996b), respectively.

In Figure 10 our final $T_{\rm effs}$ are compared with the IRFM temperatures from C11 and A96. For 47 stars in common with C11, our values are 51 K, on average, lower. In contrast, this study determined 46 K higher temperatures compared with that of A96 for 29 common stars. We note very similar statistical errors of 63 and 69 K for the temperature differences (this work—C11) and (this work—A96), respectively. Based on these comparisons, we estimate the systematic and statistical errors of $T_{\rm eff}$ for the 31 stars with the spectroscopically derived atmospheric parameters to be 50 and 70 K, respectively.

For 20 stars with the spectroscopic surface gravities, log $g_{\rm Sp}$, their *Hipparcos* parallaxes were measured with a relative parallax error less than 10%, and we calculated reliable log $g_{\rm Hip}$ values. As shown in Figure 9, log $g_{\rm Sp}$ − log $g_{\rm Hip}$ = 0.008 ± 0.037 dex. This led us to estimate the uncertainty in log $g_{\rm Sp}$ to be 0.04 dex.

Statistical error of [Fe/H] was defined by the dispersion, σ, for lines of Fe II in a given star.

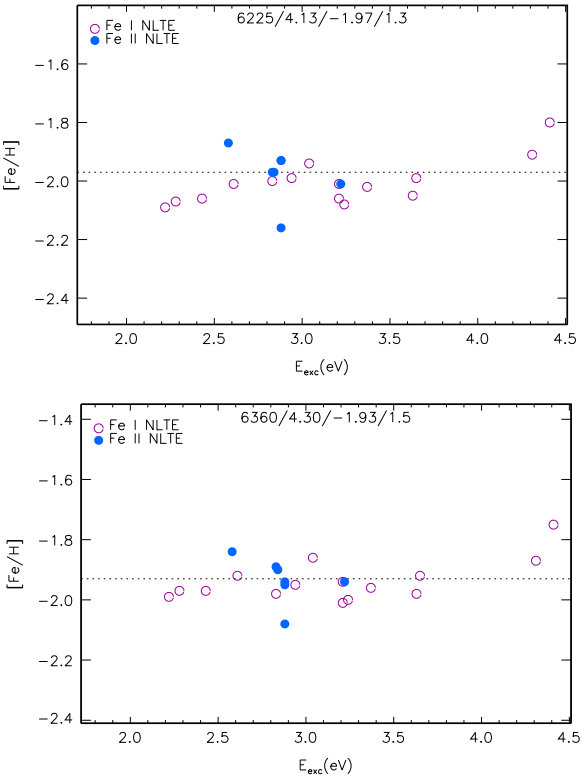

Figure 11. Impact of changes in $T_{\rm eff}$ and log g on the NLTE differential abundances derived from the Fe I (open circles) and Fe II (filled circles) lines in HD 74000. The top panel corresponds to our final parameters, $T_{\rm eff}$ = 6225 K, log g = 4.13, [Fe/H] = −1.97, and the bottom panel to $T_{\rm eff}$ = 6360 K, log g = 4.30, [Fe/H] = −1.93. The differences in NLTE abundances Fe I–Fe II = −0.03 dex and +0.01 dex, respectively.

Statistical error of the microturbulence velocity was adopted to be common for the whole stellar sample, and it was defined by the dispersion in the single ξ_t measurements about relation (2). It amounts to 0.14 km s^{-1}.

It is worth noting that the uncertainty in spectroscopically derived atmospheric parameters can be larger than that quoted above. For example, for the halo star HD 74000 we found the two sets of stellar parameters that reproduce well the Fe I/Fe II ionization and Fe I excitaion equilibrium (Figure 11) and fit the appropriate evolutionary tracks. These are $T_{\rm eff}$ = 6225 K, log g = 4.13, and [Fe/H] = −1.97, suggesting the star's age of 15 Gyr, and $T_{\rm eff}$ = 6360 K, log g = 4.30, and [Fe/H] = −1.93, resulting in τ = 13.5 Gyr. The first set relied, in fact, on $T_{\rm IRFM}$ (A96), and the second one on $T_{\rm IRFM}$(C11). A shift of +135 K in $T_{\rm eff}$ leads to +0.17 dex shift in log g, and both sets of parameters provide an acceptable star age. Neither of the two sets can be preferred from a comparison of log $g_{\rm Sp}$ with the corresponding *Hipparcos*-parallax-based surface gravity, log g_{Hip} = 4.16 ± 0.16 for $T_{\rm eff}$ = 6225 K, and log g_{Hip} = 4.20 ± 0.16 for $T_{\rm eff}$ = 6360 K. From analysis of H_α and H_β in HD 74000 Mashonkina et al. (2003) inferred $T_{\rm eff}$ = 6225 K. Two pairs of $T_{\rm eff}$/log g, which provide the Fe I/Fe II ionization equilibrium and reasonable star's mass and age, were also obtained for HD 108177 (6100/4.22/−1.67 and 6250/4.40/−1.62) and G090-003 (6100/3.90/−2.04 and 5930/3.80/−2.10). We therefore recommend applying various spectroscopic and nonspectroscopic methods to a given star to find a unique solution for the star's $T_{\rm eff}$/log g.

6. COMPARISON WITH OTHER STUDIES

For 10 stars of our sample, their $T_{\rm effs}$ were determined in the literature based on measurements of the angular diameters, trigonometric parallaxes, and bolometric fluxes. Boyajian et al. (2013, B13) published the most numerous list of the interferometric temperatures, $T_{\rm int}$, based on angular diameters measured with the CHARA array (330 m maximum baseline). Figure 10 displays the temperature differences between this study and interferometric measurements of B13, North et al. (2009), Creevey et al. (2012, 2015), and von Braun (2014). Our values are, on average, higher, with $\Delta T_{\rm eff}$ = 135 ± 126 K for 10 stars and 78 ± 81 K when excluding the two outliers, HD 103095 and HD 140283. We selected three stars for a detailed comparison.

HD 102870. Two successive determinations of Boyajian et al. (2012) and B13 resulted in $T_{\rm int}$ = 6132 and 6054 K, with small temperature errors of 36 and 13 K, respectively. A downward revision by 78 K was due to employing the different bolometric fluxes. The most recent temperature of B13 is in line with the earlier data of North et al. (2009), $T_{\rm int}$ = 6059 ± 49 K. Surface gravity based on the asteroseismic measurements amounts to log $g_{\rm seis}$ = 4.11 ± 0.02 (Creevey et al. 2013). With $T_{\rm eff}$ = 6060 K and log g = 4.11, we failed to achieve the ionization equilibrium between Fe I and Fe II and obtained Fe I–Fe II = −0.12 dex in NLTE. It is worth noting that log $g_{\rm Hip}$ = 4.14 adopted in this study agrees well with log $g_{\rm seis}$. For solar-type stars the asteroseismology method depends only weakly on $T_{\rm eff}$. Indeed, a 200 K temperature difference produces a difference of 0.007 dex in log g. To obtain consistent NLTE abundances from lines of Fe I and Fe II using log g = 4.14, one needs to have 110 K higher temperature of HD 102870 (Table 5) compared with its $T_{\rm int}$.

HD 103095. Using the CHARA array measurements, B13 and Creevey et al. (2012) derived $T_{\rm int}$ = 4771 ± 18 K and 4818 ± 54 K, respectively. We checked $T_{\rm eff}$ = 4820 K and log $g_{\rm Hip}$ = 4.60 with various spectroscopic temperature and gravity indicators.

i. The Fe I/Fe II ionization equilibrium is not fulfilled, and the NLTE abundance difference amounts to Fe I–Fe II = −0.27 dex.
ii. We compared the NLTE abundances from C I λλ9094, 9111 with the carbon abundance from a number of molecular CH bands, which are known to be sensitive to $T_{\rm eff}$ variation. The NLTE method for C I and atomic and molecular data were taken from S. Alexeeva & L. Mashonkina (2015, in preparation). With the 4820/4.60/−1.3 model, the abundance difference, C I–CH = 0.56 dex, is very large, while it amounts to −0.06 dex for our final parameters, $T_{\rm eff}$ = 5130 K and log g = 4.66.
iii. Effective temperature can also be constrained from analysis of the H_α line wings (Figure 12). The theoretical NLTE profiles of H_α were computed following Mashonkina et al. (2008). It can be seen that $T_{\rm eff}$ = 4820 K leads to shallower wings of H_α compared with the observations, but $T_{\rm eff}$ = 5130 K to a deeper core-to-wing transition region. The best fit was achieved for $T_{\rm eff}$ = 5030 K. It is worth noting that Cayrel et al. (2011) obtained, on average, 100 K lower temperatures from the H_α line wings compared with accurate effective temperatures from the apparent angular diameter for the 11

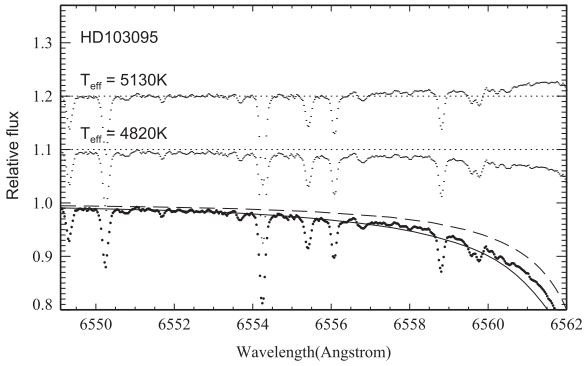

Figure 12. Theoretical NLTE flux profiles of H_α calculated with $T_{\rm eff} = 4820$ K (dashed curve) and $T_{\rm eff} = 5130$ K (solid curve) compared to the observed FOCES spectrum of HD 103095 (bold dots). The differences between observed and calculated spectra, (O–C), are shown in the upper part of the panel.

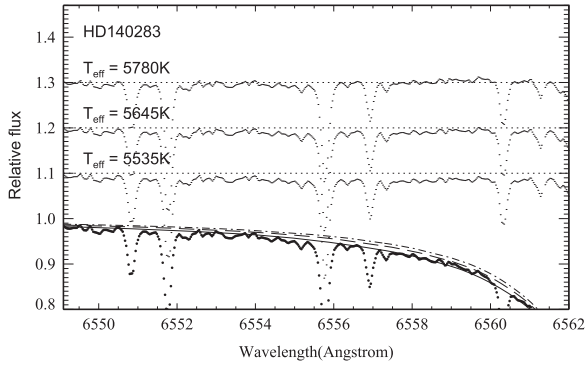

Figure 13. Theoretical NLTE flux profiles of H_α calculated with $T_{\rm eff} = 5535$ K (dot-dashed curve), 5645 K (dashed curve), and 5780 K (soild curve) compared to the observed VLT/UVES spectrum of HD 140283 (bold dots). The (O–C) values are shown in the upper part of the panel.

FGK-type stars in the $-0.7 \leqslant$ [Fe/H] $\leqslant 0.2$ range. In contrast, $T_{\rm int} = 4771$ and 4818 K of HD 103095, as determined by B13 and Creevey et al. (2012), respectively, are more than 200 K lower than the temperature from H_α.

Thus, no spectroscopic temperature indicator supports the literature data on $T_{\rm int}$ for HD 103095.

HD 140283. Creevey et al. (2015) derived $T_{\rm int} = 5534 \pm 103$ K and 5647 ± 105 K assuming zero-reddening and $A_V = 0.1^m$, respectively. It is worth noting that HD 140283 is a nearby star, at a distance of 58 pc from the Sun, and an interstellar absorption of $A_V = 0.1^m$ is unlikely produced. Of the two temperatures $T_{\rm int} = 5534$ K should be preferred; nevertheless, we checked both using the same spectroscopic indicators as for HD 103095. The NLTE abundance differences Fe I–Fe II were found to be –0.18 and –0.09 dex, respectively. For both temperatures an abundance difference between carbon atomic and molecular lines is large, with (C I–CH) = 0.69 dex and 0.32 dex, while consistent abundances, (C I–CH) = 0.00 dex, were obtained for our final parameters, $T_{\rm eff} = 5780$ K and log $g = 3.70$. Figure 13 shows theoretical profiles of H_α in the three different model atmospheres compared with the observed spectrum of HD 140283. It is evident that $T_{\rm int} = 5534$ K is too low and does not fit any spectroscopic indicator of $T_{\rm eff}$.

It is worth noting that both HD 103095 and HD 140283 have rather small angular diameters, $\theta_{\rm int} = 0.679 \pm 0.007$ mas (Creevey et al. 2012) and 0.353 ± 0.013 mas (Creevey et al. 2015), respectively, which can be overestimated, resulting in underestimated temperatures. Indeed, Casagrande et al. (2014) suspected systematic trends in the Boyajian et al. (2012, hereafter B12) data set, which was also based on the CHARA array interferometric measurements. They obtained the differences ($T_{\rm IRFM}$(C11)–$T_{\rm int}$(B12)) growing toward smaller angular diameter and reaching +200 K, on average, at $\theta_{\rm int} = 0.8$ mas.

Asteroseismic measurements of surface gravity were made for one more star of our sample, HD 49933 (Kallinger et al. 2010). They resulted in log $g_{\rm seis} = 4.22$, which is only $1.4\sigma_g$ higher than our value.

Spectroscopic stellar parameters were determined in a number of recent studies. We selected three of them for comparison. Bensby et al. (2014) used lines of Fe I and Fe II to derive temperatures and gravities of the extended stellar sample. The LTE abundances from individual lines were corrected using the grid of the NLTE abundance corrections from Lind et al. (2012). For nearby stars with very good *Hipparcos* parallaxes, Bensby et al. (2014) calculated also the log $g_{\rm Hip}$ values and found systematic discrepancies between the surface gravities from the two methods for the stars with log $g > 4.2$ and $T_{\rm eff} < 5650$ K. Therefore, they applied empirical corrections to the atmospheric parameters from ionization balance. Remember that we obtained no temperature trend of Δlog g(Sp–Hip) for our program stars (Section 5). Figure 14 (top panel) shows the differences in $T_{\rm eff}$ and log g for 17 stars in common with Bensby et al. (2014). On average, $\Delta T_{\rm eff} = -34 \pm 87$ K, Δlog $g = -0.02 \pm 0.11$, and Δ[Fe/H] $= -0.02 \pm 0.11$ in the sense "this work minus Bensby." The two independent works provide consistent stellar parameters, with the small systematic shifts and the statistical errors being typical of stellar parameter determinations. However, for some individual stars the discrepancies are uncomfortably large. For example, $\Delta T_{\rm eff}$ exceeds 100 K for five stars and Δlog $g > 0.2$ for HD 22879. We note, in particular, the differences of sign for two well-studied VMP stars HD 84937 and HD 140283, with $\Delta T_{\rm eff} = -190$ and +120 K and Δlog $g = -0.14$ and +0.13, respectively. This can be due to large uncertainty in evaluating a slope of the log A(Fe I) versus $E_{\rm exc}$ trend, where the total number of investigated lines is limited. Since the Fe I/Fe II ionization equilibrium depends on not only surface gravity but also $T_{\rm eff}$, an overestimation (underestimation) of $T_{\rm eff}$ produces an upward (downward) shift in log g.

Takeda et al. (2005) derived stellar $T_{\rm eff}$ and log g from lines of Fe I and Fe II under the LTE assumption. However, all 18 stars in common with our work lie in the $-1.3 \leqslant$ [Fe/H] $\leqslant 0.2$ metallicity range, where the departures from LTE for Fe I and Fe II are small. Therefore, the obtained differences in $T_{\rm eff}$ and log g (Figure 14, middle panel) cannot be caused by applying different line-formation treatments. The data in Figure 14 suggest, most probably, that the uncertainty in the derived effective temperature was directly translated to the uncertainty in surface gravity.

Fuhrmann (1998, 2004) applied different spectroscopic approaches to derive $T_{\rm eff}$ from the Balmer line wing fits and log g from the Mg I b line profile fits under the LTE assumption. For 16 stars in common with this work, the mean differences in effective temperature and iron abundance, $\Delta T_{\rm eff} = 29 \pm 71$ K (Figure 14, bottom panel) and Δ[Fe/H] $= 0.00 \pm 0.07$, do not exceed the error bars. HD 30743 was the only star

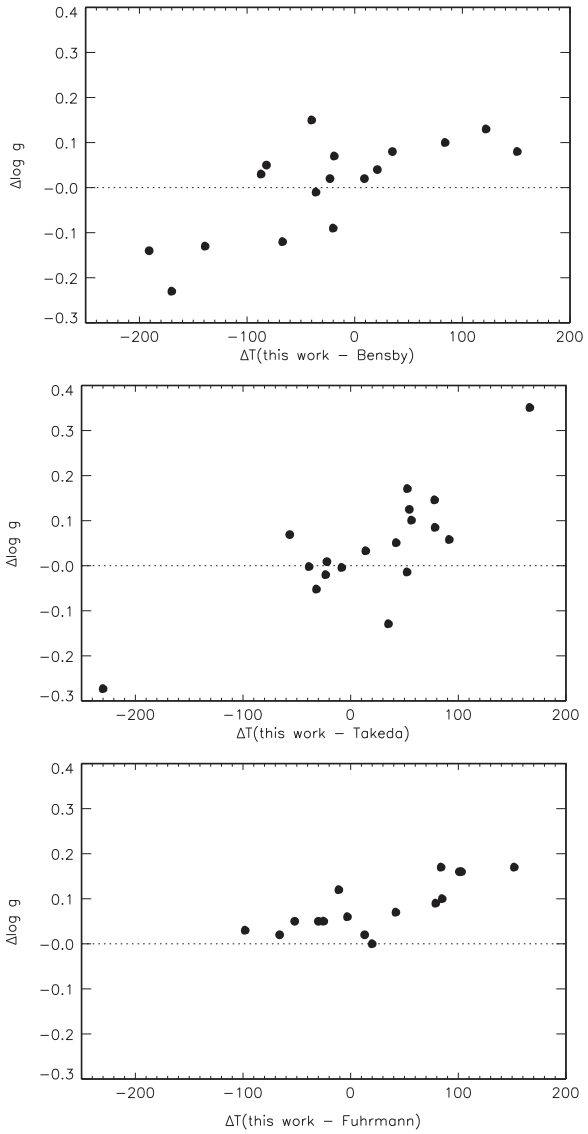

Figure 14. Differences in effective temperature and surface gravity between this study and the spectroscopic determinations by Bensby et al. (2014; top panel), Takeda et al. (2005; middle panel), and Fuhrmann (1998, 2004; bottom panel).

found with $\Delta T_{\rm eff} > 100$ K. However, this study obtains higher surface gravities, with $\Delta\log g = 0.08 \pm 0.07$. The discrepancy can be explained, in part, by using the LTE approach in Fuhrmann (1998, 2004). In the stellar parameter range, with which we are concerned, Mg I is subject to overionization, resulting in a weakened Mg I *b* line. Ignoring the departures from LTE leads to an underestimation of the derived gravity.

7. CONCLUSIONS

The sample of 51 nearby FG dwarf stars uniformly distributed over the $-2.60 <$ [Fe/H] $< +0.20$ metallicity range was selected for a systematic NLTE investigation of the Galaxy chemical evolution. Membership of individual stars to the particular galactic stellar population, namely, the thin disk, the thick disk, and the halo, was mainly identified using the star's kinematics and for a few stars using also the chemical signatures, [Fe/H] and [Mg/Fe]. A combination of the photometric and spectroscopic methods was applied to derive a homogeneous set of the stellar atmosphere parameters: $T_{\rm eff}$, log g, [Fe/H], and ξ_t. Our spectroscopic analyses took advantage of employing the high-resolution ($R \geqslant 60{,}000$) observed spectra and NLTE line formation for Fe I and Fe II in the classical 1D model atmospheres. The spectroscopic method of $T_{\rm eff}$/log g determination was tested using the 20 benchmark stars, for which there are multiple measurements of the IRFM effective temperature and their *Hipparcos* parallax error is less than 10%. An efficiency of poorly known inelastic Fe+H collisions in the SE of Fe I–Fe II was estimated empirically from analysis of their different influence on lines of Fe I and Fe II in the MP benchmark stars. We found abundances from the two ionization stages to be consistent within 0.06 dex for every star, when applying $S_{\rm H} = 0.5$.

Stellar parameters of the remaining 31 stars were obtained spectroscopically from the NLTE analysis of the iron lines. For lines of Fe II in our program stars the NLTE abundance corrections do not exceed 0.01 dex in absolute value. The deviations from LTE for Fe I grow toward higher $T_{\rm eff}$ and lower [Fe/H] and log g. For stars with either [Fe/H] $\geqslant -0.75$, or $T_{\rm eff} \leqslant$ 5750 K, or log $g \geqslant 4.20$, the difference in average abundance between NLTE and LTE was found to be less than 0.06 dex, which translates to a shift of less than 0.1 dex in log g. Since NLTE leads to weakened lines of Fe I, but it does not affect lines of Fe II until the extremely low metallicities, the ionization equilibrium Fe I/Fe II is achieved for higher gravities in NLTE than in LTE. The NLTE analysis is crucial for the VMP turnoff and subgiant stars. Indeed, the shift in log g between NLTE and LTE reaches +0.45 dex for BD−13° 3442, with $T_{\rm eff} = 6400$ K, log g(NLTE) = 3.95, and [Fe/H] = −2.62.

The obtained effective temperatures and surface gravities were checked by comparing the star's position in the log g – $T_{\rm eff}$ plane with the theoretical evolutionary track of given metallicity and α-enhancement in the Yi et al. (2004) grid. Most stars reveal self-consistent data on the star's mass, age, and kinematics.

Our final effective temperatures lie exactly in between the $T_{\rm IRFM}$ scales of A96 and C11, with a systematic shift of +46 K and −51 K, respectively. We estimate the $T_{\rm eff}$ statistical error to be about 70 K. Surface gravities obtained from the Fe I/Fe II and *Hipparcos* parallax methods were found to agree well. We do not confirm a temperature trend of $\Delta\log g$(Sp–Hip) reported by Bensby et al. (2014) for the log $g > 4.2$ and $T_{\rm eff} < 5650$ K stars.

We recommend applying a line-by-line differential approach relative to the Sun, to minimize the effect of the uncertainty in *gf*-values on the final results. It is quite efficient for the [Fe/H] > -1.5 stars. However, in the more metal-poor stars, the line-to-line scatter for Fe I has a similar magnitude for the differential and absolute abundances. This is probably due to uncertainties in C_6-values for the high-excitation lines. We note, in particular, Fe I λ5367 ($E_{\rm exc} = 4.41$ eV) and Fe I λ5383 ($E_{\rm exc} = 4.31$ eV).

It was found that none of the checked spectroscopic temperature indicators, such as Fe I versus Fe II, C I versus CH, and the H_α line wings, support interferometric effective temperatures of HD 103095, $T_{\rm int} = 4818$ K ± 54 K (Creevey et al. 2012), and HD 140283, $T_{\rm int} = 5534 \pm 103$ K (Creevey et al. 2015). Both stars have rather small angular diameters, and their measurements can be affected by some systematic trends, as suspected by Casagrande et al. (2014) for the Boyajian et al. (2012) data set.

We conclude that the NLTE analysis of lines of iron in the two ionization stages, Fe I and Fe II, is efficient in deriving reliable atmospheric parameters for the FG-type dwarf stars in the broad metallicity range, down to [Fe/H] = −2.6. The stellar parameter determinations would benefit from using the complementary data on interferometric and IRFM temperatures, trigonometric parallaxes, and asteroseismology measurements. We also recommend combining different spectroscopic temperature and gravity indicators and checking the obtained $T_{\rm eff}$/log g values with the theoretical evolutionary tracks/isochrones.

The obtained accurate atmospheric parameters will be used in the forthcoming papers to determine NLTE abundances of important astrophysical elements from lithium to europium and improve observational constraints on the chemodynamical models of the Galaxy evolution. We also plan to extend our sample toward lower metallicity and surface gravity.

The authors thank Prof. Debra Fisher for carrying out some of the observations, Oleg Kochukhov and Vadim Tsymbal for providing the codes binmag3 and synthV-NLTE at our disposal, and Klaus Fuhrmann for providing the FOCES spectra. Y.C. acknowledges the observations of the ESPaDOnS/CFHT telescope for two stars obtained through the Telescope Access Program (TAP, 2011B), which is funded by the National Astronomical Observatories. This study was supported by the Russian Foundation for Basic Research (grant 14-02-91153 and 14-02-31780), the National Natural Science Foundation of China (grants 11390371, 11233004, 11222326, 11103034, 11473033, 11473001), and the National Basic Research Program of China (grant 2014CB845701/02/03). We made use of the SIMBAD, MARCS, and VALD databases. We thank the anonymous referee for comments that helped to improve the manuscript.

REFERENCES

Adibekyan, V. Z., Figueira, P., Santos, N. C., et al. 2013, A&A, 554, A44
Allende Prieto, C., Barklem, P. S., Lambert, D. L., & Cunha, K. 2004, A&A, 420, 183
Alonso, A., Arribas, S., & Martinez-Roger, C. 1995, A&A, 297, 197
Alonso, A., Arribas, S., & Martinez-Roger, C. 1996a, A&AS, 117, 227 (A96)
Alonso, A., Arribas, S., & Martinez-Roger, C. 1996b, A&A, 313, 873
Axer, M., Fuhrmann, K., & Gehren, T. 1994, A&A, 291, 895
Bagnulo, S., Jehin, E., Ledoux, C., et al. 2003, Msngr, 114, 10
Bard, A., Kock, A., & Kock, M. 1991, A&A, 248, 315
Barklem, P. S., & Aspelund-Johansson, J. 2005, A&A, 435, 373
Barklem, P. S., Piskunov, N., & O'Mara, B. J. 2000, A&AS, 142, 467
Bensby, T., Alves-Brito, A., Oey, M. S., Yong, D., & Meléndez, J. 2010, A&A, 516, L13
Bensby, T., Feltzing, S., & Oey, M. S. 2014, A&A, 562, A71
Bergemann, M., Lind, K., Collet, R., Magic, Z., & Asplund, M. 2012, MNRAS, 427, 27
Blackwell, D. E., Ibbetson, P. A., Petford, A. D., & Shallis, M. J. 1979, MNRAS, 186, 633
Blackwell, D. E., Petford, A. D., Shallis, M. J., & Simmons, G. J. 1982a, MNRAS, 199, 43
Blackwell, D. E., Petford, A. D., & Simmons, G. J. 1982b, MNRAS, 201, 595
Bonifacio, P., Spite, M., Cayrel, R., et al. 2009, A&A, 501, 519
Boyajian, T. S., McAlister, H. A., van Belle, G., et al. 2012, ApJ, 746, 101 (B12)
Boyajian, T. S., von Braun, K., van Belle, G., et al. 2013, ApJ, 771, 40
Butler, K., & Giddings, J. 1985, in Newsletter on the Analysis of Astronomical Spectra, No 9, University of London
Carney, B. W., Latham, D. W., Laird, J. B., Grant, C. E., & Morse, J. A. 2001, AJ, 122, 3419
Casagrande, L., Ramírez, I., Meléndez, J., Bessell, M., & Asplund, M. 2010, A&A, 512, A54 (C10)
Casagrande, L., Schönrich, R., Asplund, M., et al. 2011, A&A, 530, A138 (C11)
Casagrande, L., Portinari, L., Glass, I. S., et al. 2014, MNRAS, 439, 2060
Cayrel, R., van't Veer-Menneret, C., Allard, N. F., & Stehlé, C. 2011, A&A, 531, A83
Cayrel, R., Depagne, E., Spite, M., et al. 2004, A&A, 416, 1117
Cayrel de Strobel, G., Soubiran, C., & Ralite, N. 2001, A&A, 373, 159
Chen, Y. Q., Nissen, P. E., & Zhao, G. 2004, A&A, 425, 697
Chen, Y. Q., Nissen, P. E., Zhao, G., Zhang, H. W., & Benoni, T. 2000, A&AS, 141, 491
Chiappini, C., Matteucci, F., & Romano, D. 2001, ApJ, 554, 1044
Collet, R., Asplund, M., & Trampedach, R. 2007, A&A, 469, 687
Creevey, O. L., Thevenin, F., Boyajian, T. S., et al. 2012, A&A, 545, A17
Creevey, O. L., Thevenin, F., Basu, S., et al. 2013, MNRAS, 431, 2419
Creevey, O. L., Thevenin, F., Berio, P., et al. 2015, A&A, 575, A26
de Silva, G. M., Freeman, K. C., Bland-Hawthorn, J., et al. 2015, MNRAS, 449, 2604
Dehnen, W., & Binney, J. J. 1998, MNRAS, 298, 387
Deng, L.-C., Newberg, H. J., Liu, C., et al. 2012, RAA, 12, 735
Dobrovolskas, V., Kučinskas, A., Steffen, M., et al. 2013, A&A, 559, A102
Dotter, A., Chaboyer, B., Jevremović, D., et al. 2008, ApJS, 178, 89
Drawin, H.-W. 1968, ZPhy, 211, 404
Drawin, H. W. 1969, ZPhy, 225, 483
Edvardsson, B., Andersen, J., Gustafsson, B., et al. 1993, A&A, 275, 101
Frebel, A., Casey, A. R., Jacobson, H. R., & Yu, Q. 2013, ApJ, 769, 57
Fuhrmann, K. 1998, A&A, 338, 161
Fuhrmann, K. 2000, http://www.ing.iac.es/~klaus/ (Paper II)
Fuhrmann, K. 2004, AN, 325, 3
Gehren, T., Shi, J. R., Zhang, H. W., Zhao, G., & Korn, A. J. 2006, A&A, 451, 1065
Gilmore, G., Randich, S., Asplund, M., et al. 2012, Msngr, 147, 25
González Hernández, J. I., & Bonifacio, P. 2009, A&A, 497, 497 (GB09)
Gratton, R., Carretta, E., Matteucci, F., & Sneden, C. 1996, in ASP Conf. Ser. 92, Formation of the Galactic Halo Inside and Out, ed. H. L. Morrison & A. Sarajedini (San Francisco, CA: ASP), 307
Gustafsson, B., Edvardsson, B., & Eriksson, K. 2008, A&A, 486, 951
Johnson, D. R. H., & Soderblom, D. R. 1987, AJ, 93, 864
Kallinger, T., Gruberbauer, M., Guenther, D. B., Fossati, L., & Weiss, W. W. 2010, A&A, 510, A106
Kobayashi, C., Karakas, A. I., & Umeda, H. 2011, MNRAS, 414, 3231
Kochukhov, O. 2010, http://www.astro.uu.se/~oleg/binmag.html
Kurucz, R. L. 2007, Robert L. Kurucz On-line Database of Observed and Predicted Atomic Transitions, http://kurucz.harvard.edu/atoms/2600/gf2600.pos
Kurucz, R. L., Furenlid, I., Brault, J., & Testerman, L. 1984, Solar Flux Atlas from 296 to 1300nm (New Mexico: National Solar Observatory)
Lai, D. K., Bolte, M., Johnson, J. A., et al. 2008, ApJ, 681, 1524
Lind, K., Bergemann, M., & Asplund, M. 2012, MNRAS, 427, 50
Malkin, Z. M. 2013, ARep, 57, 128
Mashonkina, L., & Gehren, T. 2000, A&A, 364, 249
Mashonkina, L., Gehren, T., Shi, J.-R., Korn, A. J., & Grupp, F. 2011, A&A, 528, A87
Mashonkina, L., Gehren, T., Travaglio, C., & Borkova, T. 2003, A&A, 397, 275
Mashonkina, L., Zhao, G., Gehren, T., et al. 2008, A&A, 478, 529
McWilliam, A., Preston, G. W., Sneden, C., & Searle, L. 1995, AJ, 109, 2757
Meléndez, J., & Barbuy, B. 2009, A&A, 497, 611
Mishenina, T. V., Soubiran, C., Kovtyukh, V. V., & Korotin, S. A. 2004, A&A, 418, 551
Nissen, P. E. 1981, A&A, 97, 145
North, J. R., Davis, J., Robertson, J. G., et al. 2009, MNRAS, 393, 245
O'Brian, T. R., Wickliffe, M. E., Lawler, J. E., Whaling, W., & Brault, J. W. 1991, JOSAB, 8, 1185
Olsen, E. H. 1983, A&AS, 54, 55
Olsen, E. H. 1993, A&AS, 102, 89
Pakhomov, Y. V., & Zhao, G. 2013, AJ, 146, 97
Raassen, A. J. J., & Uylings, P. H. M. 1998, yCat, 334, 300
Ramírez, I., Allende Prieto, C., & Lambert, D. L. 2013, ApJ, 764, 78
Ramírez, I., & Meléndez, J. 2005, ApJ, 626, 446
Randich, S., Gilmore, G., & Gaia-ESO Consortium, G. 2013, Msngr, 154, 47
Reddy, B. E., Tomkin, J., Lambert, D. L., & Allende Prieto, C. 2003, MNRAS, 340, 304
Reetz, J. K. 1991, Diploma thesis, Universität München
Romano, D., Karakas, A. I., Tosi, M., & Matteucci, F. 2010, A&A, 522, A32
Ruchti, G. R., Bergemann, M., Serenelli, A., Casagrande, L., & Lind, K. 2013, MNRAS, 429, 126
Ryabchikova, T., Fossati, L., & Shulyak, D. 2009, A&A, 506, 203

Skrutskie, M. F., Cutri, R. M., Stiening, R., et al. 2006, AJ, 131, 1163
Smiljanic, R., Korn, A. J., Bergemann, M., et al. 2014, A&A, 570, A122
Steenbock, W., & Holweger, H. 1984, A&A, 130, 319
Takeda, Y. 1994, PASJ, 46, 53
Takeda, Y., Ohkubo, M., Sato, B., Kambe, E., & Sadakane, K. 2005, PASJ, 57, 27
Tsymbal, V. 1996, in ASP Conf. Ser. 108, M.A.S.S., Model Atmospheres and Spectrum Synthesis, ed. S. J. Adelman, F. Kupka & W. W. Weiss (San Francisco, CA: ASP), 198
Turon, C., Creze, M., Egret, D., et al. 1993, BICDS, 43, 5
van Leeuwen, F. 2007, A&A, 474, 653
von Braun, K., Boyajian, T. S., van Belle, G. T., et al. 2014, MNRAS, 438, 2413
Yi, S. K., Demarque, P., & Kim, Y.-C. 2004, Ap&SS, 291, 261
Zasowski, G., Johnson, J. A., Frinchaboy, P. M., et al. 2013, AJ, 146, 81
Zhang, H. W., & Zhao, G. 2005, MNRAS, 364, 712
Zhang, H. W., & Zhao, G. 2006, A&A, 449, 127